



STATE RESEARCH CENTER OF RUSSIA
INSTITUTE FOR HIGH ENERGY PHYSICS

IHEP 2001-13

V.V. Abramov

**UNIVERSAL SCALING BEHAVIOUR
OF THE TRANSVERSE POLARIZATION
FOR INCLUSIVELY PRODUCED HYPERONS
IN HADRON-HADRON COLLISIONS**

Submitted to *European Physical Journal C*

Protvino 2001

Abstract

Abramov V.V. Universal Scaling Behaviour of the Transverse Polarization for Inclusively Produced Hyperons in Hadron-Hadron collisions: IHEP Preprint 2001-13. – Protvino, 2001. – p. 41, figs. 26, tables 12, refs.: 67.

Experimental data on the polarization of hyperons, inclusively produced in hadron-hadron collisions, have been analyzed. It is shown that the existing data can be described by a function of transverse momentum (p_T) and two scaling variables $x_{A\pm} = (x_R \pm x_F)/2$: $\mathbf{P}_H = A^\alpha F(p_T)[G(x_{A+} - x_2) - \sigma G(x_{A-} + x_2)]$. The function $G(x_{A+})$ is proportional to $\sin[\omega(x_{A+} - x_1)]/\omega$. The ω , as well as the magnitude and the sign of the hyperon polarization depend on quantum numbers of hadrons participating in a reaction. It is assumed in the analysis that wave functions of hadrons are described by the $SU(6)$ model. The atomic weight dependence of the Λ hyperon polarization is characterized by the parameter $\alpha \approx -0.16|x_F|$. There is an analogy between the scaling properties of the hyperon polarization and the analyzing power (A_N) in hadron production reactions. This new scaling law allows one to predict hyperon polarization for reactions and kinematic regions, yet unexplored in experiments and to confront these predictions with future experiments and various models.

Аннотация

Абрамов В.В. Универсальное скейлинговое поведение поперечной поляризации для инклюзивного образования гиперонов в адрон-адронных соударениях: Препринт ИФВЭ 2001-13. – Протвино, 2001. – 41 с., 26 рис., 12 табл., библиогр.: 67.

Проанализированы экспериментальные данные по поляризации гиперонов, инклюзивно образующихся в адрон-адронных соударениях. Показано, что существующие данные могут быть описаны функцией поперечного импульса (p_T) и двух скейлинговых переменных $x_{A\pm} = (x_R \pm x_F)/2$: $\mathbf{P}_H = A^\alpha F(p_T)[G(x_{A+} - x_2) - \sigma G(x_{A-} + x_2)]$. Функция $G(x_{A+})$ пропорциональна $\sin[\omega(x_{A+} - x_1)]/\omega$. Параметер ω , а также величина и знак поляризации гиперонов зависят от квантовых чисел участвующих в реакции адронов. Анализ данных проводится в предположении, что волновые функции адронов описываются $SU(6)$ моделью. Зависимость поляризации Λ гиперонов от атомного веса мишени характеризуется параметром $\alpha \approx -0.16|x_F|$. Существует аналогия между скейлинговыми свойствами поляризации гиперонов и свойствами анализирующей способности (A_N) в реакциях образования адронов. Новый скейлинг позволяет предсказать поляризацию гиперонов для реакций и кинематических областей, еще не исследованных экспериментально, и сопоставить эти предсказания с результатами будущих экспериментов и различными моделями.

Introduction

The understanding of spin-dependent effects in inclusive hadron production processes in the framework of QCD is still far from being satisfactory, despite significant experimental and theoretical progress over the past few years. In particular, the study of hyperon polarization (\mathbf{P}_H) and the analyzing power (A_N) could provide invaluable and completely new insight into the field of “spin physics” and, in addition, might also yield a better understanding of the hadronization process.

In this paper we will study the existing data for one measured spin-dependent quantity (transverse hyperon polarization \mathbf{P}_H in inclusive reactions $a + b \rightarrow c^\uparrow + X$) from an empirical point of view in collisions of unpolarized protons, antiprotons, K^\pm , π^\pm or hyperons with protons or nuclei.

Experiments on hyperon production performed during more than two decades since the first polarization observation [1] have shown that the hyperon polarization is significant in a wide range of beam energies. Almost all the existing data (with an equivalent proton momentum on a fixed target from 4 up to 2049 GeV/c) at medium and high energies are used for the analysis.

The study of Λ hyperon polarization in pp and pA collisions has been carried out in many experiments and revealed an approximate scaling behaviour as a function of x_F variable at fixed p_T , as well as a function of p_T at fixed x_F [2]-[13]. Further investigations of the hyperon polarization using different beams and targets have shown its dependence on the hyperon and the beam flavors, as well as on the target atomic weight [14]-[41]. It has to be mentioned that a large value of the hyperon polarization represents a significant problem for the existing strong interaction theory which predicts, in the framework of perturbative Quantum Chromodynamics (pQCD), the vanishing of the polarization at high p_T and energy [43]. For the review of the hyperon polarization data and the existing models see [44,45,46].

Recently a new scaling law has been proposed for a hadron production analyzing power (A_N) in reactions

$$a^\uparrow + b \rightarrow c + X$$

where a , b and c are hadrons, and the hadron a is transversely polarized [47,48]. Since the hyperon polarization and the hadron analyzing power could be closely related [49], it is reasonable to expect that similar scaling properties take place for the inclusive hyperon production in collisions of unpolarized hadron beams with protons or nuclei. According to Ref. [48] A_N at high energies (≥ 40 GeV) and high transverse momentum p_T (≥ 1 GeV/c) can be described by a simple function of two variables, p_T and x_A :

$$A_N = F(p_T)G(x_A), \quad (1)$$

where

$$x_A = p_c \cdot p_b / p_a \cdot p_b = E_c / E_a. \quad (2)$$

Here, p_c , p_b and p_a are four-momenta of the produced hadron, the target hadron and the beam hadron, respectively. The energies E_c (produced hadron) and E_a (beam hadron) are measured in a reference frame, where a polarized (p or \vec{p}) particle strikes an unpolarized target (p or A) which is at rest. There are also alternative expressions for the scaling variable x_A , which are close to (2) numerically at the high beam and secondary hadron energies [48]. In particular, neglecting masses in (2), we have in the c.m. frame

$$x_A = (x_F + x_R)/2, \quad (3)$$

where $x_F = p_z^*/p_{max}^*$ and $x_R = p^*/p_{max}^*$. Here p^* , p_z^* and p_{max}^* is momentum of the produced hadron, its longitudinal component and the maximum possible value of it, respectively, all in the c.m. reference frame. Eqs. (1) and (3) describe A_N for most of the hadron production reactions almost as well as eqs. (1) and (2) [48]. The only exception is the A_N for Λ hyperon production in $p\uparrow p(A)$ collisions, for which the variable (3) is preferable since it gives a smaller χ^2 ($\chi^2/N_{DOF} = 24.3/44$ for (3) vs $39.4/44$ for (2)), where N_{DOF} is the number of degrees of freedom in a fit. It is interesting that Λ hyperon polarization is also better described by eq. (1) if x_A is given by (3).

It has to be mentioned that the variable $x = E_c/E_a$ was used to describe the scaling properties of the secondary hadron (π, K, \bar{p}, \bar{n}) spectra in the region $E_c/E_a \geq 0.6 \div 0.7$ [50].

A natural generalization of (3) is given by a linear function of x_R and x_F variables with relative weights which could be determined from the data fit:

$$x_{A\pm} = x_R \cdot w_1 \pm x_F \cdot w_2, \quad (4)$$

where $w_1 + w_2 = 1$. For $w_1 = 0.5$ the variable x_{A+} in (4) is close to $|x_F|$ in the beam fragmentation region ($x_F \approx 1$) and $x_{A+} \approx x_T/2$ in the central region ($x_F \approx 0$). The variable x_{A-} have similar properties in the backward hemisphere ($x_F \leq 0$). For $w_1 = 0.5$ variable x_{A+} is identical to x_A (eq.(3)).

The hyperon polarization features are different in some respects from the analyzing power features listed in [48]. In particular, we have to take into account that the polarization of hyperons produced in pp collisions is antisymmetric in x_F by virtue of rotational invariance [11,51]:

$$\mathbf{P}_H(x_F, p_T) = -\mathbf{P}_H(-x_F, p_T) \quad (5)$$

From the relation (5) we have also for the hyperon polarization $\mathbf{P}_H(0, p_T) = 0$ in contrast to the analyzing power, which could be different from zero even at $x_F = 0$ [48].

From a dimensional analysis alone, the polarization \mathbf{P}_H admits two types of contributions, which are functions of u/s and t/s :

$$\mathbf{P}_H = F(p_T) \left[G_+(-u/s) - G_-(-t/s) \right], \quad (6)$$

where u , t and s are Mandelstam variables:

$$\begin{aligned} s &= (p_a + p_b)^2 \approx +2p_a \cdot p_b, \\ t &= (p_a - p_c)^2 \approx -2p_a \cdot p_c, \\ u &= (p_b - p_c)^2 \approx -2p_b \cdot p_c, \end{aligned} \quad (7)$$

where in the last column the hadron masses are neglected. It is easy to show that at high energies the following approximations are valid:

$$-u/s \approx (x_R + x_F)/2 = x_{A+}, \quad (8)$$

$$-t/s \approx (x_R - x_F)/2 = x_{A-}, \quad (9)$$

where $x_{A\pm}$ are given by eq. (4) with $w_1 = 0.5$. Relations, similar to (8)-(9), have been used in Refs. [52,53]. Using eqs. (7) - (9) it is easy to show that $x_{A+} \approx p_c \cdot p_b / p_a \cdot p_b = x_A$, where x_A is given by eq. (2).

The expression, which takes into account (5)-(9) and other features of \mathbf{P}_H is given below:

$$\mathbf{P}_H = A^\alpha F(p_T)[G(x_{A+} - x_2) - \sigma G(x_{A-} + x_2)], \quad (10)$$

where an additional phase x_2 and a normalization parameter σ are introduced to take into account a possible violation of (5) for collisions, different from pp one (for pp collisions $x_2 \equiv 0$ and $\sigma \equiv 1$). It is assumed below that $\sigma = 1$ for pA collisions, while x_2 could be different from zero. The functions $F(p_T)$ and $G(x_{A\pm})$ are determined below from the experimental data.

Exactly the same approach can be used to derive an expression for the A_N . The difference is that in the last case $G_+(x) \neq G_-(x)$ in (6), and $G_+(x_{A+})$ dominates, as the data fit show, over $G_-(x_{A-})$.

For the process $pp(A) \rightarrow \Lambda + X$ we use the expression

$$F(p_T) = 1 - e^{-\kappa p_T^3} \quad (11)$$

for the $F(p_T)$, where κ is a fit parameter and p_T is measured in GeV/c. The other processes may require a different expression. The exact shape of the $F(p_T)$ should be measured in future experiments. For the $G(x_{A\pm})$ we use an expression

$$G(x_{A\pm}) = \frac{c}{2\omega} \cdot \sin[\omega(x_{A\pm} - x_1)], \quad (12)$$

similar to the one, used in [48], which takes into account such a feature of \mathbf{P}_Λ , as an approximate linear dependence on the x_F . The difference of eq. (12) from the corresponding expression in [48] is that the former has an additional factor $1/(2\omega)$, that makes parameters c and ω less correlated and reflects the tendency of hyperon polarization magnitude decrease with ω rise. The parameters w_1 , c , x_1 , x_2 , σ and ω are determined from the data.

The Λ polarization data fits indicate that both parameters x_1 and x_2 can depend on p_T and only at high enough $p_T \geq 1.5$ GeV/c are compatible with p_T -independent constant values:

$$x_1 = \eta_0 - \eta_1 e^{-\delta p_T^3}, \quad (13)$$

$$x_2 = (1 - Z/A)(\xi_0 - \xi_1 e^{-\nu p_T^3}), \quad (14)$$

where the target dependent factor $(1 - Z/A)$ is introduced to insure $x_2 = 0$ for pp collisions, as required by relation (5). For a neutron target $Z/A = 0$, so the phase x_2 is the only parameter in the above equations which makes the hyperon polarization for the proton target different from that of the neutron one. This feature of eq. (14) can be used to estimate the difference in the polarization of hyperons produced on the proton and the neutron targets.

The factor A^α takes into account a possible atomic weight dependence of the hyperon polarization. The α could be a constant or a function of kinematic variables:

$$\alpha = \alpha_1|x_F| + \alpha_0, \quad (15)$$

where α_0 and α_1 are fit parameters.

In the beam fragmentation region $x_R \approx x_F$, and $x_{A+} \approx x_F$, while $x_{A-} \approx 0$. So, in this region the dependence of eq. (10) on x_F is determined, mainly, by the first term $G(x_{A+} - x_2) \approx G(x_F - x_2)$. The second term in (10), $G(x_{A-} + x_2) \approx G(x_2)$ has a weak x_F dependence. In the target fragmentation region x_F dependence is determined, mainly, by the $\sigma G(x_{A-} + x_2) \approx \sigma G(-x_F + x_2)$.

Eq. (10) for $\sigma = \pm 1$ can be expressed using (12) in a different way, with the explicit x_R and x_F dependences:

$$\mathbf{P}_H = \frac{c}{\omega} A^\alpha \cdot F(p_T) \begin{cases} \cos[\omega(x_R w_1 - x_1)] \sin[\omega(x_F w_2 - x_2)], & \text{if } \sigma = +1; \\ \sin[\omega(x_R w_1 - x_1)] \cos[\omega(x_F w_2 - x_2)], & \text{if } \sigma = -1. \end{cases} \quad (16)$$

Eq. (10) has a more general form, but it coincides with (16) if we choose eq. (12) for $G(x_{A\pm})$ and set $\sigma = \pm 1$. The magnitude of the hyperon polarization is about cA^α/ω . It is assumed here that $F(p_T)$ is equal unity at its maximum.

In case of the analyzing power measurements we have a non-zero contribution to the left-right asymmetry from the polarized hadron (beam or target) only and the feature (5) is not valid. Naively, we may say that only the first term, $G(x_{A+} - x_2)$, in (10), corresponding to a polarized beam, gives a non-zero contribution to the analyzing power and, as a result, we have eq. (1) for it. For the case of Λ hyperon polarization in the pp collisions both terms in (10), corresponding to the beam fragmentation and the target fragmentation, have non-zero contributions and cancel each other at $x_F = 0$, in accordance to (5).

Relation (5) is not valid in general for collisions of different hadrons, like $K^-p(A)$ or $\bar{p}p$ collisions. In these cases we have to use different functions $G_+(x_{A+})$ and $G_-(x_{A-})$ of x_{A+} and x_{A-} , respectively. In particular, parameter x_2 can be different from zero and σ can be different from unity.

It should be also mentioned, that in the case of a linear function $G(x_{A\pm})$ and $\sigma = 1$ in (10) the polarization \mathbf{P}_H is a function of x_F only (at fixed p_T) due to the cancellation of x_R terms in (10). The use of $\sin(x)$ in (12) makes $G(x_{A\pm})$ non-linear, that prevents complete cancellation of x_R terms in (10). A linear case corresponds to the limit $\omega \rightarrow 0$ in the above equations, while the data fits give for $pp(A) \rightarrow \Lambda + X$ process $\omega \approx 3$, indicating a rather non-linear behaviour of $G(x_{A\pm})$ at large values of arguments. As we will see in the following sections the ω can be expressed for different reactions via a linear combination of terms, which are functions of quantum numbers characterizing the particular reaction (see eq. (22)). Eq. (22) is used below to fix the ω in eq. (10) in data fits that allows us to estimate the other parameters with a better accuracy.

It follows from eqs. (10) - (15) that for the hp collisions the hyperon polarization \mathbf{P}_H and the analyzing power A_N obey the Helmholtz equation:

$$\frac{\partial^2 \mathbf{P}_H}{\partial x_{A+}^2} + \frac{\partial^2 \mathbf{P}_H}{\partial x_{A-}^2} + \omega^2 \mathbf{P}_H = 0. \quad (17)$$

Eq. (17) reflects the non-linearity of the \mathbf{P}_H dependence on scaling variables $x_{A\pm}$, which is characterized by the ω parameter.

Most of the hyperon production experiments have been performed on nuclear targets, where relation (5) may not be exactly valid. Also, practically all the available data are concentrated in the forward hemisphere. We cannot exclude that future measurements in the backward hemisphere (nuclear target fragmentation region) will show some deviation from (15), which will require a correction of the polarization A -dependence. An estimate of nuclear effects in the forward hemisphere will be given below on the base of existing data. We assume also for simplicity that the ω parameter in the same for the forward and the backward hemispheres.

1. Lambda hyperon polarization in pp and pA collisions

The dependence of Λ polarization (\mathbf{P}_Λ) vs x_F for the Λ production in $pp(A)$ collisions [2]-[13] is shown in Fig. 1. The data shown in Fig. 1 include proton collisions with protons and different nuclei (d, Be, Cu, W and Pb).

We assume here that for the positive polarization the hyperon spin is directed along the unit vector $\vec{n} \equiv \vec{p}_a \times \vec{p}_c / |\vec{p}_a \times \vec{p}_c|$, which is the normal to the production plane. Here, \vec{p}_a and \vec{p}_c is a momentum of the beam hadron and that of the produced hyperon, respectively.

The fit parameters for eqs. (10)-(15) are shown in Table 1 for different data samples and fit conditions.

Table 1. Fit parameters of eqs. (10)-(15) for Λ production in $pp(A)$ collisions. Different fit conditions are explained in the text.

Fit #	1	2	3	4	5
c	-1.22 ± 0.05	-1.22 ± 0.09	-1.22 ± 0.05	-1.23 ± 0.05	-1.15 ± 0.05
ω	3.13 ± 0.24	3.29 ± 0.38	3.045	1.22 ± 0.30	0.93 ± 0.38
σ	1.0	1.03 ± 0.09	1.0	0.0	0.0
w_1	0.5	0.51 ± 0.05	0.5	0.20 ± 0.03	0.0
η_0	0.406 ± 0.023	0.404 ± 0.034	0.412 ± 0.017	0.097 ± 0.020	0.068 ± 0.021
η_1	0.31 ± 0.14	0.29 ± 0.14	0.33 ± 0.14	0.30 ± 0.06	0.32 ± 0.06
δ	4.7 ± 1.6	4.6 ± 1.7	4.7 ± 1.7	4.4 ± 1.2	4.3 ± 1.2
ξ_0	0.075 ± 0.011	0.077 ± 0.025	0.075 ± 0.011	0.103 ± 0.032	0.133 ± 0.035
ξ_1	0.213 ± 0.043	0.218 ± 0.061	0.213 ± 0.042	0.212 ± 0.060	0.244 ± 0.064
ν	1.26 ± 0.22	1.26 ± 0.23	1.24 ± 0.22	0.81 ± 0.23	0.79 ± 0.21
κ	1.89 ± 0.14	1.89 ± 0.15	1.88 ± 0.13	1.78 ± 0.15	1.64 ± 0.14
α_0	0.0	-0.01 ± 0.03	0.0	0.0	0.0
α_1	-0.154 ± 0.016	-0.133 ± 0.053	-0.156 ± 0.015	-0.153 ± 0.016	-0.123 ± 0.015
χ^2/N_{DOF}	$325.9/259$	$325.7/256$	$326.0/260$	$322.9/258$	$354.6/259$

A fit # 1 uses the data for all the targets (shown in Fig. 1). For the fit # 1 all the parameters are free except $\alpha_0 = 0$, $w_1 = 0.5$ and $\sigma = 1$ in accordance with the expectations from eqs. (6)-(9). The use of p_T -dependent phases x_1 and x_2 in eqs. (13)-(14) improves the fit quality significantly (χ^2/N_{DOF} changed from 1.81 to 1.26). The absolute value of x_2 is small in accordance with the approximate validity of the feature (5) for pA collisions.

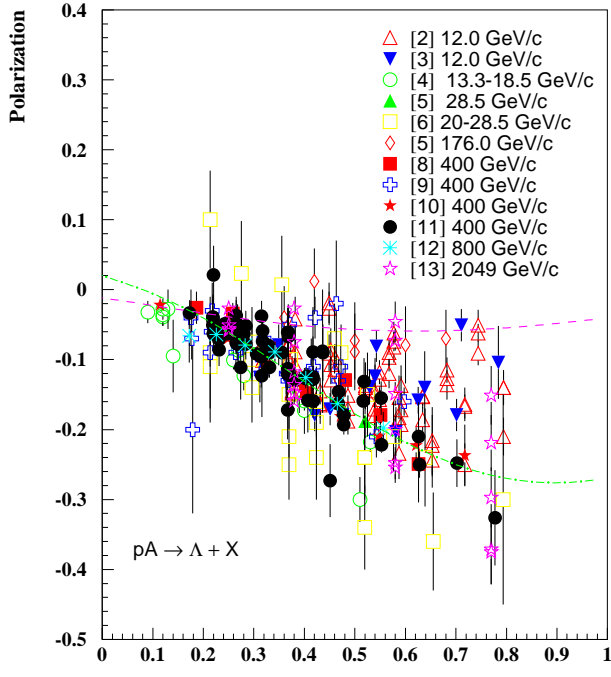


Fig. 1. Polarization vs x_F for Λ production in $pp(A)$ collisions. The fit parameters of eqs. (10)-(15) are presented in Table 1, fit # 3. The curves correspond to fit predictions (12) for $p_T = 0.5$ GeV/c (dashed) and $p_T = 1.5$ GeV/c (dash-dotted), respectively.

An interesting feature of the above fits is that at the first approximation the α is proportional to $|x_F|$. The higher is a hyperon momentum the more its polarization is attenuated by the interactions with a nuclear target. For a heavy nuclear target and a large x_F we expect a significant attenuation of the polarization in comparison with the pp collisions case. In particular, for $x_F = 0.7$ we have $\alpha = -0.15|x_F| = 0.105$ and the polarization on a Lead target is reduced by a factor $A^{-0.105} = 0.57$. On a Beryllium target a corresponding factor is 0.79. A similar order of magnitude for the polarization degradation in complex nuclei can be found in [44], where it is also shown that the polarization degradation is p_T -independent.

By setting $\sigma = 0$ in (10) we can reduce this equation to a form similar to eq. (1) which was used to fit the analyzing power data in Refs. [47,48]. The fit # 4 is made with $\sigma = 0$ and $\alpha_0 = 0$ while the other parameters are free, including the weight w_1 in eq. (4). The fit # 4 gives as good data approximation as the fit # 2, with $\chi^2/N_{DOF} = 1.25$. The “effective” scaling variable (x_{A+}) in the forward hemisphere, where practically all the existing data were measured, is given according to the fit # 4 by the relation $x_{A+} = 0.2x_R + 0.8x_F$. Though the fit quality is good enough for the $x_F \geq 0$ data, eq. (10) with parameters, corresponding to the fit # 4 does not have the feature (5) even for pp collisions. We expect that future data for $x_F \leq 0$ region will not be approximated well enough by the fit # 4. That is the reason why eq. (10) with $\sigma \approx 1$ is preferable for the description of the Λ polarization scaling properties. It is interesting that most of the parameters have very similar values for the fits # 3 and # 4. The stability of the fit parameters makes predictions following from eq. (10) more reliable.

For a fit # 2 all the parameters are free. The values of $w_1 = 0.51 \pm 0.06$ and $\sigma = 1.03 \pm 0.09$ for the fit # 2 are close to the expected ones (0.5 and 1, respectively) with practically the same $\chi^2/N_{DOF} = 1.27$. So, the fit # 2 supports the choice of scaling variables in the form $x_{A\pm} = (x_R \pm x_F)/2$ and an approximate rotational asymmetry (5) for the polarization in $pp(A)$ collisions, though the experimental data exist only in the forward hemisphere.

The parameters ω and α_0 are close in the fit # 2 to 3 and zero, respectively. The fit # 3 is made with four parameters fixed ($\omega = 3.045$, $\sigma = 1$, $w_1 = 0.5$ and $\alpha_0 = 0$) that simplifies eq. (10) and allows one to determine the other parameters with a better accuracy. Predictions for the \mathbf{P}_Λ dependence on x_F from eqs. (11)-(15) with the fit # 3 parameters are shown in Fig. 1 for 400 GeV/c pBe collisions. The dashed line corresponds to $p_T = 0.5$ GeV/c, and the dash-dotted line corresponds to $p_T = 1.5$ GeV/c. Most of the data points are situated between these two curves. At high p_T (≥ 1.5 GeV/c) the position of maximum in $|\mathbf{P}_\Lambda|$ is near $x_F \approx 0.8 - 0.9$, while at lower p_T it is located at smaller x_F values.

The results of the above fits (# 1 - # 4) indicate that the variable x_F alone is not the best one for approximation of the Λ polarization scaling properties in $pp(A)$ collisions, and the use of two variables (x_F and x_R or $x_{A\pm}$) gives a better result. The direct check of a possible pure x_F scaling is done in the fit # 5, where $\sigma = 0$ and $w_1 = 0$. That excludes the x_R variable from eq. (10). The χ^2 for the fit # 5 is significantly higher with $\chi^2/N_{DOF} = 1.37$.

The p_T dependence of \mathbf{P}_Λ is described by the function $F(p_T)$, which is sharply rising for $p_T \leq 1.2$ GeV/c and is practically constant for higher p_T . The experimental dependence of \mathbf{P}_Λ on p_T is illustrated in Fig. 2, where the ratio of \mathbf{P}_Λ and $A^\alpha D(x_{A+}, x_{A-})$ is shown, and

$$D(x_{A+}, x_{A-}) = G(x_{A+} - x_2) - \sigma G(x_{A-} + x_2). \quad (18)$$

The ratio is assumed to be a function of p_T only. An additional cut $x_F \geq 0.35$ is used for the data shown in Fig. 2 to exclude the points with large fractional errors of the ratio. The data in Fig. 2 show the independence of the ratio on the beam energy, x_F and the target type, and confirms the scaling behaviour and factorization of the p_T and $x_{A\pm}$ dependencies, assumed in (10). New measurements are desirable for $p_T \geq 1.5$ GeV/c to clarify the \mathbf{P}_Λ and $F(p_T)$ behaviour at high p_T .

A detailed comparison of the fit # 3 with the most precise polarization data is illustrated in Figs. 3, 4 and 5.

Fig. 3 represents the data from experiments [10,11] and [12], performed in pBe collisions at 400 and 800 GeV/c. The fitting curves reproduce the x_F dependence, as well as small variations of it with p_T .

In Fig. 4 the fitting curves are compared with the pp data [13] at the beam equivalent momentum 2049 GeV/c for $p_T = 0.6$ GeV/c, 0.76 GeV/c and 1.26 GeV/c, respectively. The values of \mathbf{P}_Λ differ very much for these three values of p_T and the corresponding fitting curves (fit # 3) reproduce these features of the data.

The attenuation of the Λ polarization on nuclear targets and the dependence of the attenuation on x_F are illustrated in Fig. 5. The measured polarization is divided by $F(p_T)D(x_{A+}, x_{A-})$ and the corresponding ratio is plotted in Fig. 5 vs x_F . The most precise data for the pp [13], pBe [11], and pW [3] collisions show a decrease of polarization on Be and W targets with x_F rise in comparison with the proton-proton collisions case. The existing \mathbf{P}_Λ data on medium and heavy nuclear targets are limited in terms of their accuracy and kinematic range. Additional measurements on medium and heavy nuclear targets for positive and negative x_F are desirable to confirm and clarify the polarization attenuation effects, shown in Fig. 5. It will be interesting also to measure the A -dependence of the analyzing power A_N and compare it with that of the hyperon polarization.

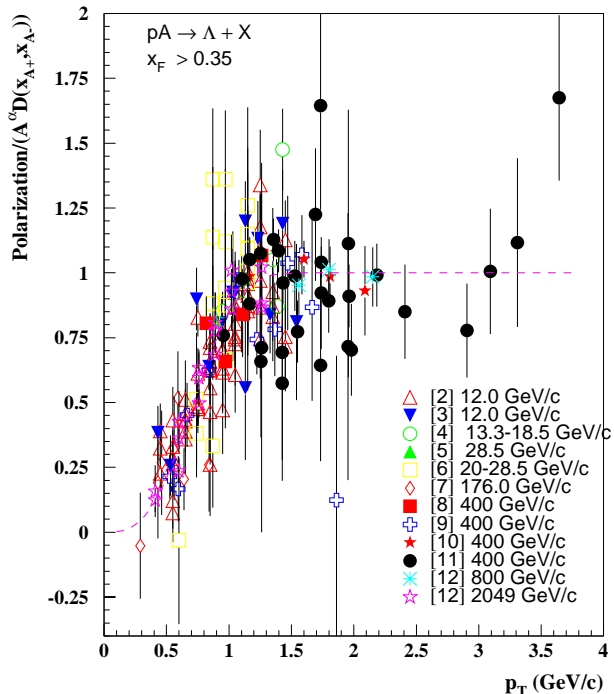


Fig. 2. The ratio of polarization and $A^\alpha D(x_{A+}, x_{A-})$, (eq. (17)) vs p_T for Λ production in $pp(A)$ collisions, and $x_F \geq 0.35$. Parameters of eqs. (10)-(15) are presented in Table 1, fit # 3. The curve corresponds to the function $F(p_T)$ in eq. (10).

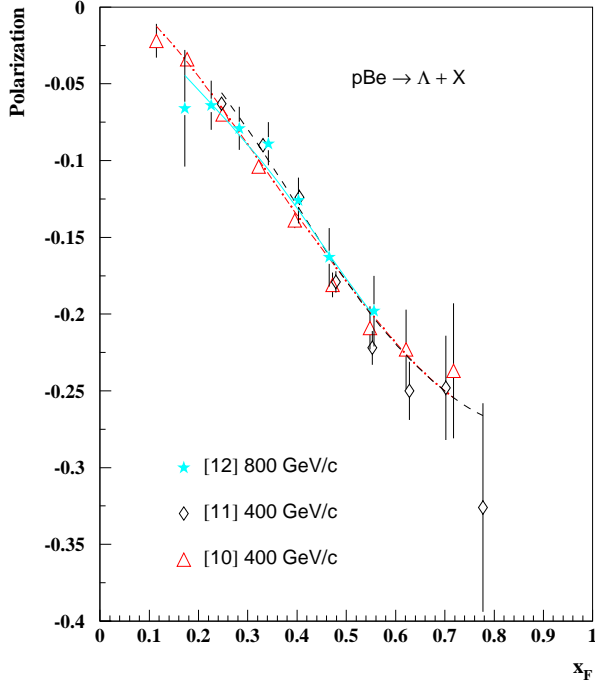


Fig. 3. Polarization vs x_F for Λ production in $p - Be$ collisions. The fit parameters of eq. (10) are presented in Table 1, fit # 3. The fitting curves correspond to data [12] (solid), [11] (dashed), and [10] (dash-dotted), respectively.

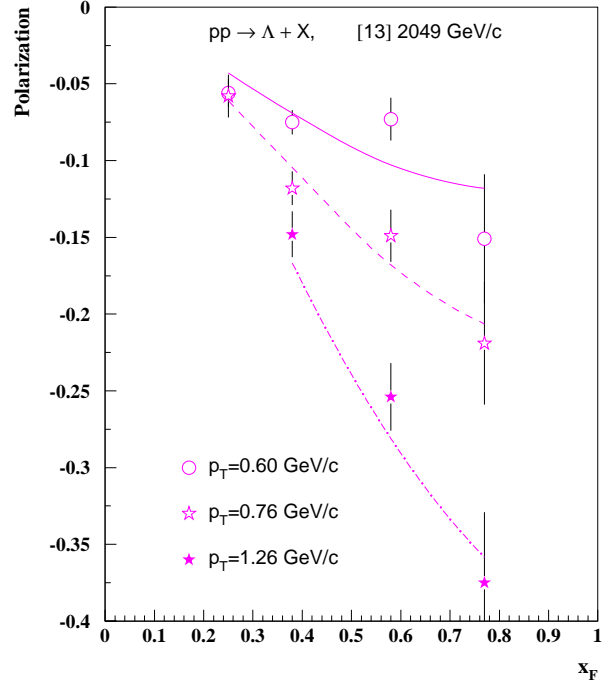


Fig. 4. Polarization vs x_F for Λ production in pp collisions [11]. The fit parameters of eq. (10) are presented in Table 1, fit # 3. The fitting curves correspond to data [13] for $p_T = 0.6$ GeV/c (solid), 0.76 GeV/c (dashed), and 1.26 GeV/c (dash-dotted), respectively.

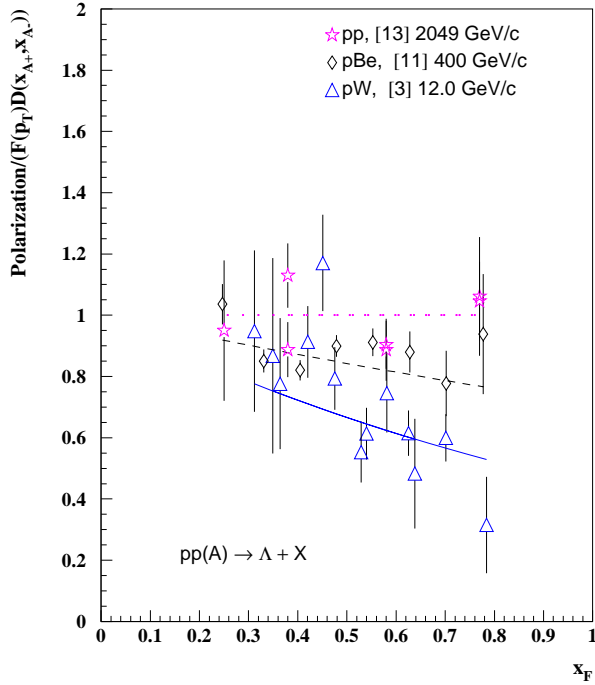


Fig. 5. The ratio of polarization and $F(p_T)D(x_{A+}, x_{A-})$ (see eqs. (10),(12), (17)) vs x_F for Λ production in pp [13], pBe [11] and pW [3] collisions. Parameters of eqs. (10)-(15) are presented in Table 1, fit # 3. The curves correspond to the pp (dotted), pBe (dashed) and pW (solid) collisions, respectively.

The general agreement between the data and the fits # 1 - # 3 can be considered a good one, taking into account statistical and possible systematic errors of the data in different experiments.

We may conclude that Λ polarization reveals a scaling behaviour, when it is presented in a forward hemisphere as a function of two scaling variables $x_{A\pm}$ (or x_R and x_F) and p_T . The use of a single scaling variable (g.e. x_F) and p_T does not allow one to describe the data well enough.

2. Polarization of $\Sigma^{\pm,0}$ and $\Xi^{0,-}$ hyperons in pp and pA collisions

In this section the polarization of $\Sigma^{\pm,0}$ and $\Xi^{0,-}$ hyperons in pp and pA collisions is analyzed. The corresponding fit parameters are presented in Tables 2 and 3. The fits have been performed using eqs. (10)-(15), and eq.

$$F(p_T) = \begin{cases} p_T/p_T^0, & \text{if } p_T \leq p_T^0; \\ 1, & \text{otherwise;} \end{cases} \quad (19)$$

for the function $F(p_T)$, which is found to be more appropriate for an approximation of the polarization dependence on p_T . For this section and all the following the parameters α_0 and w_1 are fixed ($\alpha_0 = 0$ and $w_1 = 0.5$).

Table 2. Fit parameters of eqs. (10)-(19) for Σ^{\pm} production in $pp(A)$ collisions.

Fit #	1	2	3	4
H	Σ^+	Σ^+	Σ^-	Σ^-
c	4.4 ± 1.0	4.0 ± 0.9	4.2 ± 2.5	4.2 ± 4.2
ω	1.9 ± 1.2	3.045	6.1 ± 4.0	6.090
σ	1.0	1.0	1.0	1.0
p_T^0	1.21 ± 0.07	1.24 ± 0.06	0.66	0.66
η_0	-0.10 ± 0.31	0.107 ± 0.059	0.25	0.25 ± 0.20
η_1	-0.56 ± 0.79	-0.22 ± 0.62	0.0	0.0
δ	4.7 ± 7.5	5 ± 19	0.0	0.0
ξ_0	0.337 ± 0.015	0.341 ± 0.013	0.307 ± 0.058	0.31 ± 0.11
ξ_1	0.172 ± 0.054	0.198 ± 0.044	0.0	0.0
ν	0.82 ± 0.28	0.98 ± 0.20	0.0	0.0
α_1	-0.26 ± 0.05	-0.24 ± 0.04	-0.26	-0.26
χ^2/N_{DOF}	33.0/17	33.6/18	0.06/3	0.06/3

Table 3. Fit parameters of eqs. (10)-(19) for $\Xi^{-,0}$ production in $pp(A)$ collisions.

Fit #	1	2	3	4
H	Ξ^-	Ξ^-	Ξ^0	Ξ^0
c	-0.81 ± 0.12	-0.81 ± 0.12	-1.37 ± 0.50	-1.37 ± 0.61
ω	5.95 ± 0.74	6.090	6.10 ± 0.92	6.090
σ	1.0	1.0	1.0	1.0
p_T^0	0.4 ± 0.2	0.4 ± 0.3	0.5	0.5
η_0	0.29 ± 0.11	0.284 ± 0.073	0.336 ± 0.023	0.336 ± 0.036
η_1	-0.030 ± 0.082	-0.033 ± 0.060	0.0	0.0
δ	2 ± 12	2.5 ± 9.7	0.0	0.0
ξ_0	0.00 ± 0.22	0.02 ± 0.13	-0.2	-0.20 ± 0.15
ξ_1	0.51 ± 0.12	0.50 ± 0.10	0.0	0.0
ν	3.0 ± 1.9	2.9 ± 1.5	0.0	0.0
α_1	0.03 ± 0.14	0.04 ± 0.11	-0.12	-0.12
χ^2/N_{DOF}	71.0/46	71.0/47	5.7/13	5.7/13

2.1. The Σ^+ hyperon polarization

The polarization of Σ^+ hyperons (\mathbf{P}_{Σ^+}) in pA collisions has been measured on a Cu target at 800 GeV/c [14] and on a Cu and a Be targets at 400 GeV [15,16,8]. The dependence of \mathbf{P}_{Σ^+} on x_F is shown in Fig. 6. A fit # 1 corresponds to the Σ^+ data, shown in Fig. 6, with some parameters fixed due to a limited data statistics. The x_F position of the polarization maximum rises with p_T and at $p_T = 1.5$ GeV/c it is near $x_F = 0.8$. The parameter $\omega = 1.9 \pm 1.2$ is compatible with the value of ω for the case of Λ polarization discussed in the previous section. The fit # 2 is done with the value of $\omega = 3.045$, which follows from eq. (22).

The dependence of \mathbf{P}_{Σ^+} on p_T is illustrated in Fig. 7, where a ratio of \mathbf{P}_{Σ^+} and $A^\alpha D(x_{A+}, x_{A-})$ is plotted. The curve corresponds to the function $F(p_T)$ in eq. (19) with $p_T^0 \approx 1.2$ GeV/c (fit # 2). The function $F(p_T)$ is well approximated by a linear dependence for $p_T \leq 1.2$ GeV/c and a plateau for higher p_T (see Fig. 7), but additional measurements are desirable for higher p_T and different x_F .

It was stated in [14] that the Σ^+ polarization at 800 GeV/c decreases as a function of p_T at fixed x_F . The results of the fit # 2 indicate that such unusual p_T dependence is probably due to the p_T dependence of the parameter x_2 in eq. (14). As we can see from eq. (16), the polarization (for $\sigma = 1$) is proportional to $\sin[\omega(x_F w_2 - x_2)] \approx \sin[3(x_F/2 - x_2)]$. Since $x_2 \approx (1 - Z/A)(0.34 - 0.17e^{-0.82p_T^2})$ and $(1 - Z/A) \approx 0.4$, the value of x_2 is about 0.09 for $p_T \leq 0.5$ GeV/c, it starts to grow fast for $0.5 \leq p_T \leq 1.5$ GeV/c, and has a plateau $x_2 \approx 0.19$ for higher p_T values. The value of x_F in [14] is about 0.46, so $\mathbf{P}_{\Sigma^+} \propto \sin[3(0.23 - x_2)]$ and decreases with p_T rise for $p_T \geq 0.7$ GeV/c. This decrease of $D(x_{A+}, x_{A-})$ is not compensated

by a corresponding increase of the $F(p_T)$, that leads to the observed polarization decrease with p_T rise. If we take $x_F \geq 0.65$, such effect as a decrease of polarization with p_T increasing is not expected (see Fig. 6). The results of three other Σ^+ polarization measurements, which have typical $x_F \geq 0.52$, do not reveal a decrease of \mathbf{P}_{Σ^+} with p_T rise [15,16,8].

It was also stated in [14] that an energy dependence of \mathbf{P}_{Σ^+} is observed by comparing the results at 800 GeV/c (*Cu* target) [14], at 400 GeV/c (*Be* target) [15] and 400 GeV/c (*Cu* target) [16]. The observed difference is really due to the different targets (*Cu* vs *Be*) and slightly different x_F values used for this comparison. In the case of comparison of the data on *Be* and *Cu* targets a strong A dependence is the reason of a higher polarization on the *Be* target, since $\alpha = -0.26|x_F|$ (see fit # 1). For the data on *Cu* target [16] the corresponding $x_F \approx 0.52$ and $\mathbf{P}_{\Sigma^+} = 0.168 \pm 0.017$, while the 800 GeV/c data are measured at $x_F \approx 0.46$ and $\mathbf{P}_{\Sigma^+} = 0.124 \pm 0.001$. The data [15] and the fitting curve for $p_T = 1.5$ GeV/c in Fig. 6 show that the \mathbf{P}_{Σ^+} increases by 0.05 or more, when x_F is increased from 0.47 to 0.52. So, the expected \mathbf{P}_{Σ^+} for 800 GeV/c and $x_F = 0.52$ is about $0.124 + 0.05 = 0.174$, which is compatible with the measured value $\mathbf{P}_{\Sigma^+} = 0.168 \pm 0.017$ at 400 GeV/c.

The energy independence of the polarization is confirmed by Fig. 7, where all the data points at two beam energies and two different targets are approximated well by a single function $F(p_T)$ and are compatible with the scaling law (10), described using p_T and two scaling variables x_{A+} and x_{A-} .

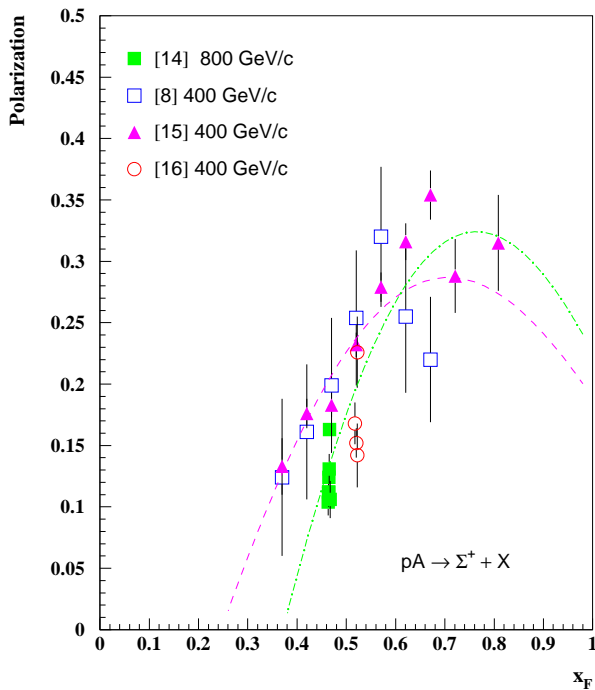


Fig. 6. Polarization vs x_F for Σ^+ production in pA collisions. The fit parameters of eqs. (10)-(19) are presented in Table 2. The curves corresponds to the fit # 2 predictions for $p_T = 0.8$ GeV/c (dashed) and $p_T = 1.5$ GeV/c (dash-dotted), respectively.

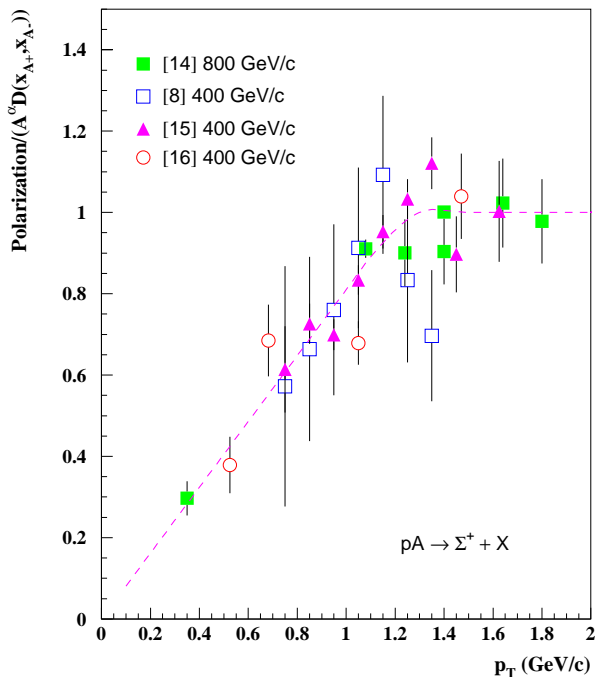


Fig. 7. The ratio of polarization and $A^\alpha D(x_{A+}, x_{A-})$, (eq. (17)) vs p_T for Σ^+ production in pA collisions. Parameters of eqs. (11)-(19) are presented in Table 2, fit # 2. The curve corresponds to the function $F(p_T)$ in eq. (18).

The data fit indicates also that Σ^+ polarization decreases on a nuclear target ($\propto A^{-0.26|x_F|}$). The polarization attenuation is more significant at high $|x_F|$ values, similar to that of for the Λ hyperons.

We may conclude that the use of two scaling variables (x_{A+} and x_{A-}) in the form of eq. (10) instead of one (x_F) resolves the problem of energy dependence of the Σ^+ polarization and the problem of its unusual p_T dependence (see details in [14]), and presents the existing data in the energy independent way.

2.2. The Σ^- hyperon polarization

The polarization of Σ^- (\mathbf{P}_{Σ^-}) has been measured at 400 GeV/c in pCu [17] and pBe [18] collisions. Since just a few points in x_F and p_T has been measured, some of the fit # 3 parameters are fixed, see Table 2. In addition, for the fit # 4 the ω parameter was fixed: $\omega = 6.090$ (see Table 2). The x_F dependence of \mathbf{P}_{Σ^-} is plotted in Fig. 8 vs x_F . It has a maximum near $x_F \approx 0.67$ with corresponding $\omega \approx 6$. The p_T dependence indicates some flattening of the function $F(p_T)$ above 0.7 GeV/c and shows a good agreement of the data on Be and Cu targets.

2.3. The Σ^0 hyperon polarization

The polarization of Σ^0 (\mathbf{P}_{Σ^0}) produced in pBe has been measured at 28.5 GeV/c [5] and at 18.5 GeV/c [19]. Only two data points are available from these two experiments. At 28.5 GeV/c the value of \mathbf{P}_{Σ^0} is 0.28 ± 0.13 ($x_F = 0.6$, $p_T = 1.01$ GeV/c), and at 18.5 GeV/c it is 0.23 ± 0.13 ($0 < x_F < 0.75$, $0.5 < p_T < 2$ GeV/c), which is consistent with the Σ^\pm polarization in the same kinematic area.

2.4. The Ξ^- hyperon polarization

The polarization of Ξ^- (\mathbf{P}_{Ξ^-}) has been measured at 800 GeV/c in pBe [20,21] collisions, and at 400 GeV/c in pCu [22] and pBe [23] collisions. The fit # 1 is made with some parameters fixed. The value of parameter ω is found to be compatible with 6. In the fit # 2 the $\omega = 6.090$ is used and the corresponding curves are shown in Fig. 9 for $p_T = 0.5$ GeV/c (dashed line), and $p_T = 1.5$ GeV/c (dash-dotted line) for 400 GeV/c pBe collisions.

The fit # 2 and Fig. 9 data indicate a local maximum in the absolute value of polarization at x_F in the range 0.3-0.6, depending on p_T value.

The A -dependence of the \mathbf{P}_{Ξ^-} is not significant ($\alpha_1 \approx 0.04 \pm 0.11$).

2.5. The Ξ^0 hyperon polarization

The polarization of Ξ^0 (\mathbf{P}_{Ξ^0}) has been measured at 400 GeV/c in pBe [9] collisions. The data are presented in Fig. 10 vs x_F . Due to a small number of experimental points some of the fit parameters were fixed near the values which give the best χ^2 . The fit # 3 is done with the ω free and the fit # 4 - with $\omega = 6.090$.

The fit # 4 and Fig. 10 data indicate a local maximum in the absolute value of polarization near $x_F \approx 0.4$.

The fits # 2 and # 4 indicate a possible decrease in the absolute value of \mathbf{P}_{Ξ^0} and \mathbf{P}_{Ξ^-} for $x_F \geq 0.6 - 0.8$ due to a high value of $\omega \approx 6$. This feature makes these reactions different from the Λ production in pA collisions, discussed above.

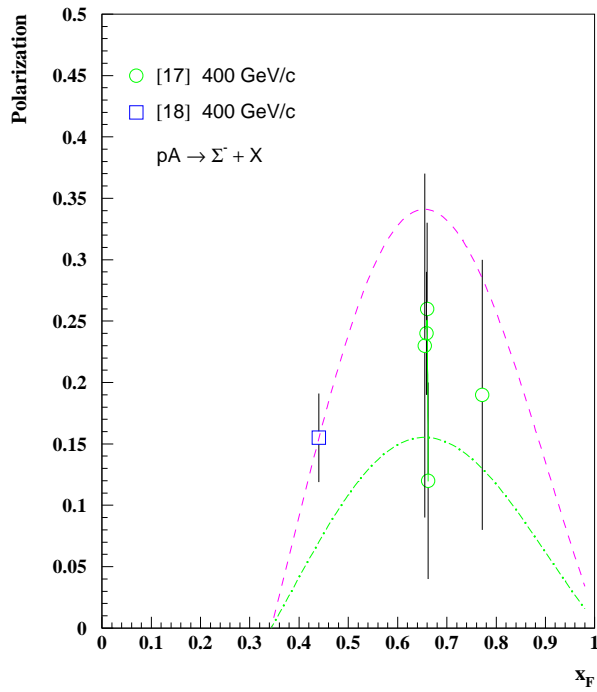


Fig. 8. Polarization vs x_F for Σ^- production in pA collisions. Parameters of eqs. (11)-(19) are presented in Table 2, fit # 4. The curve corresponds to the function $F(p_T)$ in eq. (17).

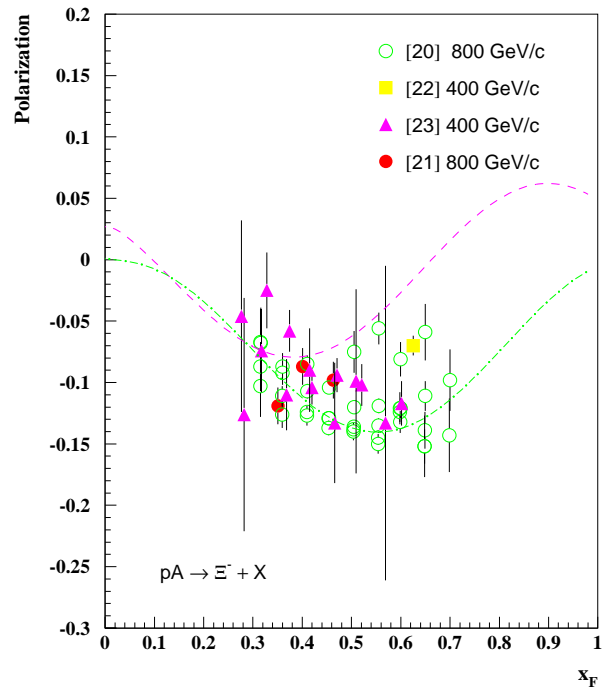
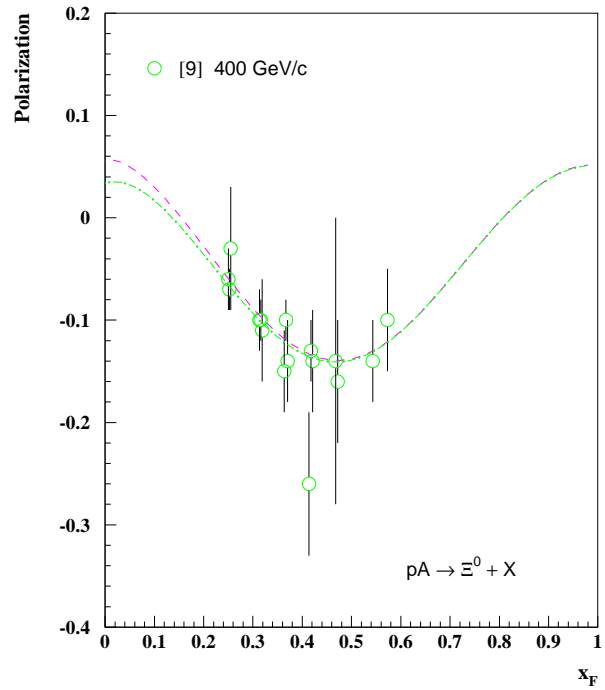


Fig. 9. Polarization vs x_F for Ξ^- production in pA collisions. The fit parameters of eqs. (10)-(19) are presented in Table 3. The curves correspond to the fit # 2 for $p_T = 0.5$ GeV/c (dashed), and $p_T = 1.5$ GeV/c (dash-dotted), respectively.

Fig. 10. Polarization vs x_F for Ξ^0 production in pA collisions. The fit parameters of eqs. (10)-(19) are presented in Table 3. The curves correspond to the fit # 4 for $p_T = 0.5$ GeV/c (dashed), and $p_T = 1.5$ GeV/c (dash-dotted), respectively.



An interesting observation follows from the analysis of the scaling properties of hyperon (Λ , Σ^\pm , Ξ^- and Ξ^0) polarization in $pp(A)$ collisions - the parameter ω (“polarization oscillation frequency”) in eqs. (10)-(19), which describes the rate of change of the polarization with $x_{A\pm}$ increase, is related with the number of sea quarks (N_{SEA}), picked up from the sea during a hyperon production: $\omega \approx 3N_{SEA}$.

3. Polarization of Λ , Ξ^- and $\bar{\Lambda}$ hyperons produced in K^-p collisions

In this section we analyze the hyperon polarization data in K^-p collisions. The corresponding fit parameters are presented in Table 4. Since the initial state (K^-p) is not symmetric vs the rotation transformation and there are no measurements on nuclear targets, some modification of eqs. (10)-(19) is introduced. In particular, the parameters α_0 , α_1 are fixed at zero values, $w_1 = 0.5$, and the factor $(1 - Z/A)$ in eq. (14) is omitted:

$$x_2 = \xi_0 - \xi_1 e^{-\varepsilon p_T^3}. \quad (20)$$

The function $F(p_T)$ is given by eq. (19). The σ parameter in (10) could be different from unity due to an asymmetric initial state.

Table 4. Fit parameters of eqs. (10)-(20) for Λ , Ξ^- and $\bar{\Lambda}$ production in K^-p collisions.

Fit #	1	2	3	4	5
H	Λ	Λ	Ξ^-	Ξ^-	Λ
c	4.18 ± 0.47	4.25 ± 0.37	6.0 ± 2.8	6.8 ± 2.7	10 ± 10
ω	3.53 ± 0.22	3.58	3.04 ± 0.88	3.58	5.55
σ	-0.77 ± 0.12	-0.77 ± 0.11	-0.90 ± 0.67	-1.09 ± 0.51	-0.5
p_T^0	1.0	1.0	1.0	1.0	1.0
η_0	0.076 ± 0.019	0.079 ± 0.016	0.127 ± 0.049	0.142 ± 0.038	0.14 ± 0.05
η_1	0.81 ± 0.21	0.80 ± 0.20	-0.01 ± 0.13	-0.046 ± 0.065	0.0
δ	26	26	26	26	0.0
ξ_0	0.191 ± 0.063	0.19 ± 0.06	0.06 ± 0.16	0.09 ± 0.08	0.25
ξ_1	0.18 ± 0.13	0.19 ± 0.11	-0.42 ± 0.22	-0.34 ± 0.12	0.0
ν	7	7	27	27	0.0
χ^2/N_{DOF}	$88.8/55$	$88.9/56$	$12.9/11$	$13.3/12$	$0.00/0$

3.1. The Λ polarization in K^-p collisions

The polarization of Λ (\mathbf{P}_Λ) hyperons in K^-p collisions has been measured at 176 GeV/c [7], at 32 GeV/c [24], at 14.3 GeV/c [25,26], and at 10 and 16 GeV/c [27]. The data with lower beam momenta are not used for this analysis due to the energy dependence of the polarization below 9 GeV/c at fixed negative x_F [24,25,26,28]. The interesting feature of these K^- beam

data is that they include both, the beam and the target fragmentation regions. That feature allows us to estimate the σ parameter in eq. (10) and check that the scaling behaviour is valid for both hemispheres.

Only the data with $|x_F| \leq 0.90$ are used for this analysis to avoid a large contribution of exclusive channels near the kinematic limits. The dependence of \mathbf{P}_Λ vs x_F is shown in Fig. 11, where fit predictions are also shown. The curves are calculated for $p_T = 0.3$ (dashed line) and $p_T = 0.7$ (dash-dotted line) and can be considered as envelopes for the presented data points.

The data fits (# 1 and # 2) have been performed with some parameters fixed due to a limited statistics. In the fit # 1 the parameter ω is free, and in the fit # 2 its value is fixed at $\omega = 3.58$. Both fits have χ^2/N_{DOF} about 1.6 and indicate the maximum near $x_F = 0.7$ and almost x_F -independent polarization for the negative x_F region. The σ parameter is *negative* in contrast to the pp data. The data fits indicate an oscillation of the \mathbf{P}_Λ as a function of x_F which is illustrated by the curves in Fig. 11. The magnitude and the phase of the oscillation depend on p_T .

The p_T dependence of the \mathbf{P}_Λ is compatible with a linear rise of the $F(p_T)$ (see eq. (19)) for $p_T \leq 0.85$ GeV/c.

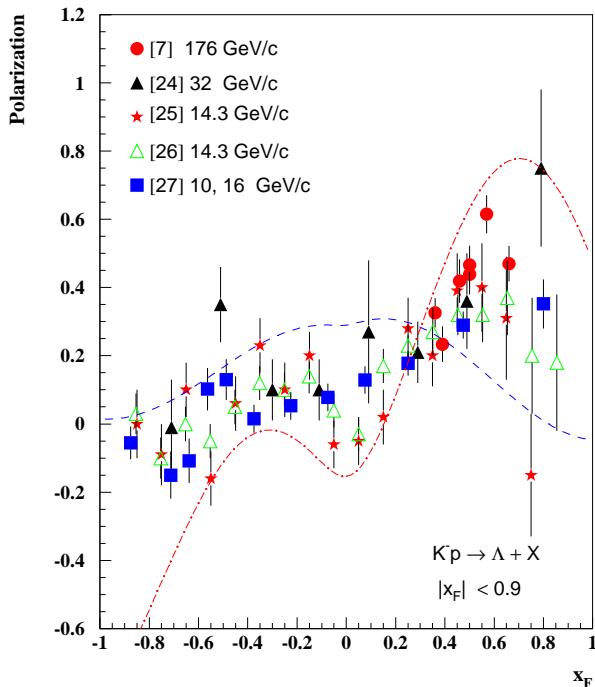


Fig. 11. Polarization vs x_F for Λ production in K^-p collisions. The fit parameters of eqs. (10)-(20) are presented in Table 4. The curves correspond to the fit # 2 for $p_T = 0.3$ GeV/c (dashed line), and $p_T = 0.7$ GeV/c (dash-dotted line), both at the beam momentum 176 GeV/c.

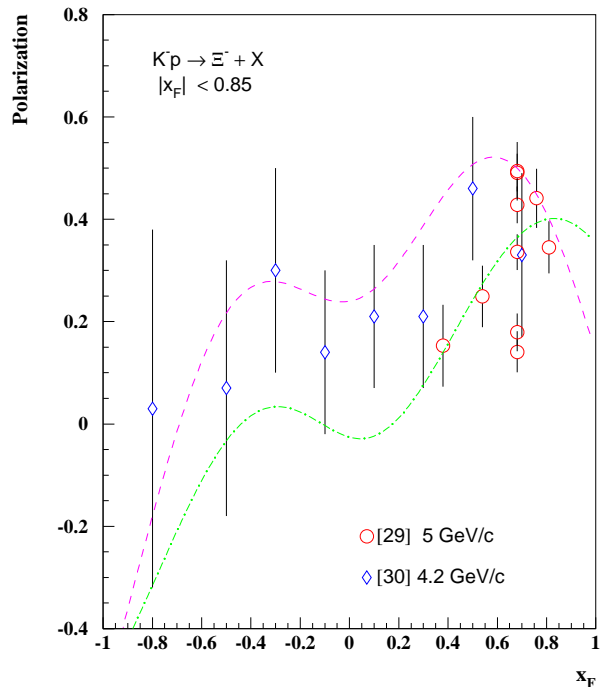


Fig. 12. Polarization vs x_F for Ξ^- production in K^-p collisions. The fit parameters of eqs. (10)-(20) are presented in Table 4. The curves correspond to the fit # 4 for $p_T = 0.5$ GeV/c (dashed line), and $p_T = 0.3$ GeV/c (dash-dotted line), respectively.

3.2. The Ξ^- polarization in K^-p collisions

The polarization of Ξ^- (\mathbf{P}_{Ξ^-}) hyperons in K^-p has been studied at 5 GeV/c [29] and at 4.2 GeV/c [30]. Since the polarization in [29] is integrated over one of the variables (x_F or p_T), we have to assign mean values for these integrated variables. As estimates of these mean values we take for the analysis $\langle x_F \rangle = 0.6$, and $\langle p_T \rangle = 0.3$ GeV/c, respectively. The dependence of \mathbf{P}_{Ξ^-} on x_F is shown in Fig. 12 along with the fit predictions for $p_T = 0.3$ GeV/c and $p_T = 0.5$ GeV/c, respectively. The predictions are made for 5 GeV/c K^-p collisions. Only data with $|x_F| \leq 0.85$ are used for the analysis to exclude the resonance region, in particular in the extreme forward region ($x_F \approx 1$) which is dominated by the baryon exchange process $K^-p \rightarrow \Lambda\pi^0$. The fit # 3 is made with the ω parameter free, and the fit # 4 is made for $\omega = 3.58$. Both fits show a maximum of \mathbf{P}_{Ξ^-} at $x_F \approx 0.6 - 0.8$ and near zero polarization for $x_F \leq 0$. The fits reproduce well the main features of the data. As in the case of the Λ polarization the σ parameter is negative, but with a much larger uncertainty.

Additional measurements are desirable for $p_T \geq 0.5$ GeV/c where polarization could reach high values. Both, the x_F and the p_T dependencies of \mathbf{P}_{Ξ^-} are similar to the case of the Λ polarization in K^-p collisions.

3.3. The $\bar{\Lambda}$ polarization in K^-p collisions

The $\bar{\Lambda}$ polarization in K^-p collisions has been measured at 32 GeV/c [24]. Since just two x_F points are available, most of parameters of eqs. (10)- (20) in the fit # 5 were fixed, with only the c and the ξ_0 - free. The $\omega = 5.55$ is taken as predicted by eq. (22). The results of the fit are presented in Table 4. Much more data are desirable for this reaction.

4. Hyperon polarization in K^+p collisions

The hyperon polarization data for K^+p collisions have been analyzed using eqs. (10)- (20). Only the data with $|x_F| \leq 0.74$ are used for the analysis. The fit parameters are presented in Table 5.

Table 5. Fit parameters of eqs. (10)-(20) for Λ , and $\bar{\Lambda}$ production in K^+p collisions.

Fit #	1	2	3	4
H	Λ	Λ	Λ	Λ
c	-3.0 ± 1.9	-2.4 ± 1.3	3.4 ± 1.1	3.9 ± 1.0
ω	4.4 ± 1.5	3.58	4.4 ± 1.9	5.55
σ	0.30 ± 0.18	0.36 ± 0.28	-1.24 ± 0.39	-1.40 ± 0.28
p_T^0	0.4	0.4	0.4	0.4
η_0	-0.19 ± 0.13	-0.21 ± 0.13	0.12 ± 0.07	0.130 ± 0.049
η_1	0.0	0.0	0.24 ± 0.35	0.29 ± 0.30
δ	0.0	0.0	17 ± 28	17 ± 20
ξ_0	-0.53 ± 0.31	-0.73 ± 0.24	0.41 ± 0.22	0.42 ± 0.16
ξ_1	0.0	0.0	0.54 ± 0.32	0.53 ± 0.17
ν	0.0	0.0	5.7 ± 5.7	4.3 ± 2.7
χ^2/N_{DOF}	9.6/12	9.8/13	12.4/19	13.0/20

4.1. The Λ polarization in K^+p collisions

The Λ polarization in K^+p collisions has been measured at 8.2 and 16 GeV/c [31], at 13 GeV/c [32], and at 32 GeV/c [24]. The fit # 1 is made with the ω parameter free, and the fit # 2 - with the $\omega = 3.58$. The dependence of polarization vs x_F is shown in Fig. 13 along with the fit # 2 predictions for $p_T = 0.3$ GeV/c and $p_T = 0.5$ GeV/c. The polarization does not depend on energy and has a maximum near $x_F = 0.35$.

4.2. The $\bar{\Lambda}$ polarization in K^+p collisions

The $\bar{\Lambda}$ polarization in K^+p collisions has been measured at 32 and 70 GeV/c [33], at 8.2 and 16 GeV/c [31], at 32 GeV/c [24], and at 13 GeV/c [32]. The data [33] for 32 and 70 GeV/c are combined for this analysis and an average momentum 50 GeV/c is assigned to it. The fit # 3 and the fit # 4 have been performed with ω parameter free and fixed ($\omega = 5.55$), respectively. The fits result in a negative $\sigma \approx -1$, similar to the $K^-p \rightarrow \Lambda$ case. The fits indicate the existence of significant phases x_1 and x_2 , which depend on p_T . The hyperon polarization observed in this reaction is higher than in any other one.

The dependence of $\bar{\Lambda}$ polarization on x_F is shown in Fig. 14 along with the fit # 4 predictions for $p_T = 0.5$ GeV/c and $p_T = 0.7$ GeV/c. The $\bar{\Lambda}$ polarization increases sharply above $x_F = 0.2$ and is about 0.8 at its maximum.

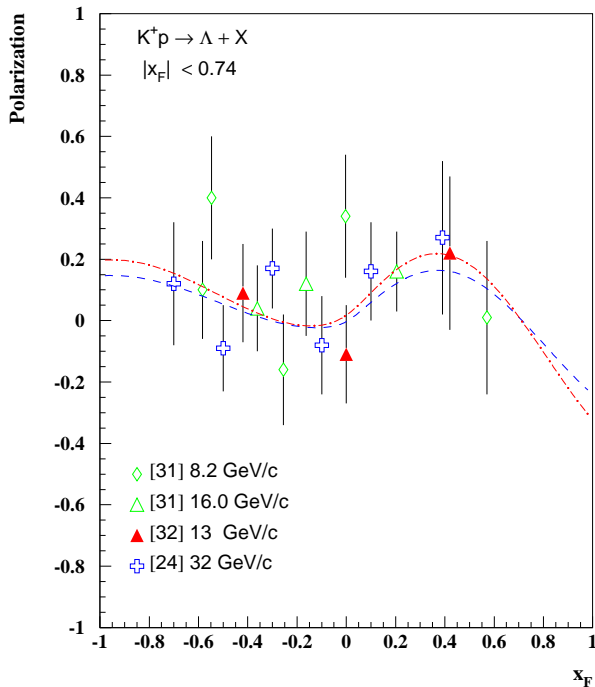


Fig. 13. Polarization vs x_F for Λ production in K^+p collisions. The fit parameters of eqs. (10)-(20) are presented in Table 5. The curves correspond to the fit # 2 for $p_T = 0.5$ GeV/c (dashed line), and $p_T = 0.3$ GeV/c (dash-dotted line), respectively.

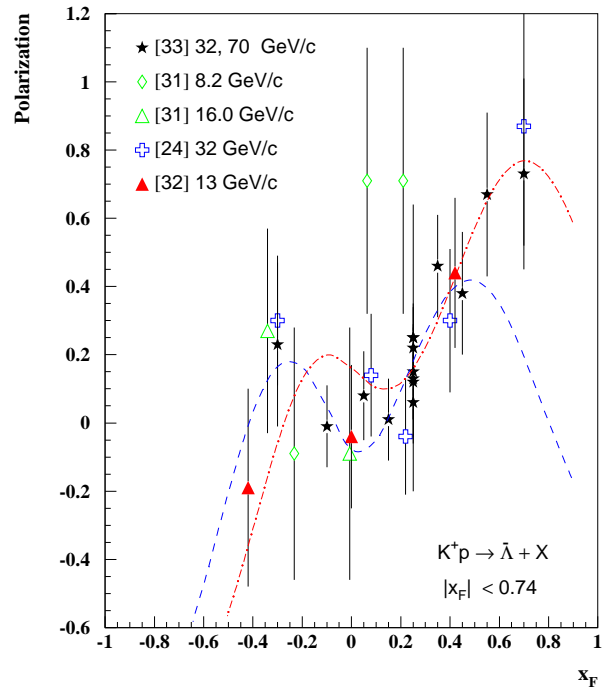


Fig. 14. Polarization vs x_F for $\bar{\Lambda}$ production in K^+p collisions. The fit parameters of eqs. (10)-(20) are presented in Table 5. The curves correspond to the fit # 4 for $p_T = 0.5$ GeV/c (dashed), and $p_T = 0.7$ GeV/c (dash-dotted), respectively.

5. The Λ polarization in π^-p and π^+p collisions

The hyperon polarization data for $\pi^\pm p$ collisions have been analyzed using eqs. (10)- (20). The fit parameters are presented in Table 6. A cut $|x_F| \leq 0.74$ is used to reduce exclusive reaction contributions.

Table 6. Fit parameters of eqs. (10)-(20) for Λ production in $\pi^\pm p$ collisions.

Fit #	1	2	3	4
Beam	π^-	π^-	π^+	π^+
c	-1.8 ± 0.5	-1.7 ± 0.6	-2.2 ± 2.2	-2.5 ± 2.9
ω	4.33 ± 0.94	3.58	5.2 ± 6.5	3.58
σ	1.0	1.0	1.5	1.5
p_T^0	1.0	1.0	1.0	1.0
η_0	0.564 ± 0.088	0.632 ± 0.081	0.45 ± 0.46	0.64 ± 0.10
η_1	2.0 ± 2.1	2.5 ± 1.0	0.0	0.0
δ	50 ± 35	49 ± 16	0.0	0.0
ξ_0	0.276 ± 0.044	0.264 ± 0.048	-0.14 ± 0.70	-0.35 ± 0.23
ξ_1	0.45 ± 0.47	0.50 ± 0.43	0.9	0.9
ν	12 ± 11	13 ± 11	1.0	1.0
χ^2/N_{DOF}	20.9/19	21.2/20	0.40/3	0.42/4

5.1. The Λ polarization in π^-p collisions

The Λ polarization in π^-p collisions has been measured at 3.95 GeV/c [34], at 6 GeV/c [35], at 15 GeV/c [36], at 16.1 GeV/c [37] and at 18.5 GeV/c [38]. The fit # 1 is made with the ω parameter free and the fit # 2 is performed with the $\omega = 3.58$. The x_F dependence of polarization is shown in Fig. 15 along with fit predictions for $p_T = 0.5$ GeV/c and $p_T = 0.7$ GeV/c. The polarization is positive in the target fragmentation region and is negative or near zero for positive x_F .

5.2. The Λ polarization in π^+p collisions

The Λ polarization in π^+p collisions has been measured at 18.5 GeV/c [38]. The fit # 3 is made with the ω parameter free and the fit # 4 is made with the $\omega = 3.58$. The data and the fit predictions for $p_T = 0.5$ GeV/c and $p_T = 0.7$ GeV/c are shown in Fig. 16.

The polarization magnitude for Λ hyperons produced in $\pi^\pm p$ collisions is smaller than it is in the pp collisions.

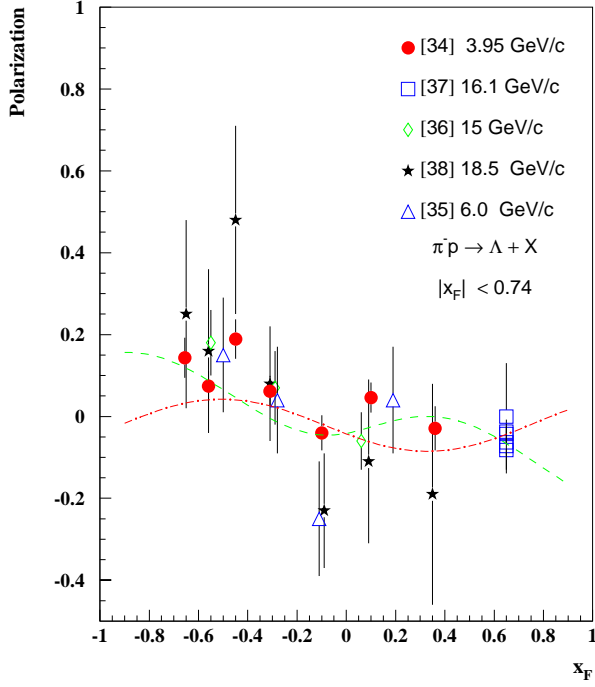


Fig. 15. Polarization vs x_F for Λ production in $\pi^- p$ collisions. The fit parameters of eqs. (10)-(20) are presented in Table 6. The curves correspond to the fit # 2 for $p_T = 0.5$ GeV/c (dashed), and $p_T = 0.7$ GeV/c (dash-dotted), respectively.

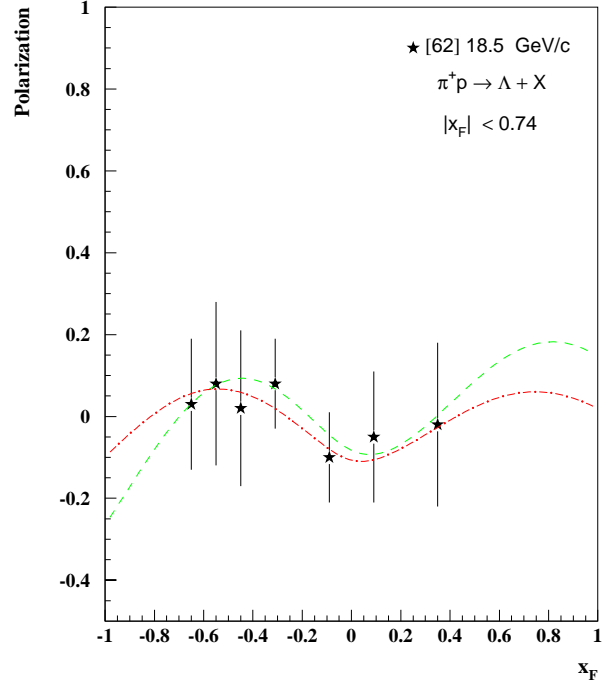


Fig. 16. Polarization vs x_F for Λ production in $\pi^+ p$ collisions. The fit parameters of eqs. (10)-(20) are presented in Table 6. The curves correspond to the fit # 4 for $p_T = 0.5$ GeV/c (dashed), and $p_T = 0.7$ GeV/c (dash-dotted), respectively.

Table 7. Fit parameters of eqs. (10)-(20) for reactions $pp \rightarrow \bar{\Lambda} + X$, $pp \rightarrow \bar{\Xi}^+ + X$, and $\bar{p}p \rightarrow \bar{\Lambda} + X$.

Fit #	1	2	3	4	5	6
<i>Process</i>	$pA \rightarrow \Lambda$	$pA \rightarrow \Lambda$	$pA \rightarrow \bar{\Xi}^+$	$pA \rightarrow \bar{\Xi}^+$	$\bar{p}A \rightarrow \Lambda$	$\bar{p}A \rightarrow \Lambda$
c	-0.47 ± 0.23	-0.49 ± 0.22	-25 ± 270	-16 ± 12	4.5 ± 2.9	3.5 ± 1.2
ω	18.5 ± 5.7	22.27	64 ± 22	65.19	16.2 ± 4.1	14.21
σ	1	1	1	1	-1	-1
p_T^0	0.34	0.34	0.4	0.4	0.6 ± 0.9	0.4 ± 0.6
η_0	0.185 ± 0.029	0.174 ± 0.015	0.045	0.045 ± 0.007	0.071 ± 0.061	0.042 ± 0.016
η_1	0.31	0.31	0.0	0.0	0.0	0.0
δ	3.7 ± 1.9	4.3 ± 1.1	0.0	0.0	0.0	0.0
ξ_0	0.309 ± 0.072	0.322 ± 0.077	0.17 ± 0.11	0.181 ± 0.007	0.294 ± 0.020	0.303 ± 0.021
ξ_1	0.07 ± 0.15	0.10 ± 0.16	0.0	0.0	0.0	0.0
ν	1.27	1.27	0.0	0.0	0.0	0.0
χ^2/N_{DOF}	12.9/16	13.3/17	0.00/0	0.00/0	0.74/2	1.08/3

6. Polarization of antihyperons produced using baryon and antibaryon beams

The reactions presented in this section can be considered as exotic ones due to a very unusual behaviour of the corresponding polarization with the rise of scaling variables. This behaviour cannot be predicted by the existing models. Most of the theoretical models predict zero polarization for antihyperon production in $pp(A)$ collision since they do not have valence quarks common with the beam or target hadrons. The recent experiments have revealed non-zero polarization for $\bar{\Xi}^+$ [21] and $\bar{\Sigma}^-$ [14] hyperons. Other antihyperons also indicate non-zero polarizations with small but not negligible magnitudes.

The fit parameters are presented in Table 7. The α parameter in eq. (10) is set to zero due to a limited statistics and too few used targets.

6.1. Polarization of $\bar{\Lambda}$ in pA collisions

The $\bar{\Lambda}$ polarization have been measured in pBe collisions at 400 GeV/c [10,11] and at 800 GeV/c [12].

Although the magnitude of the polarization is very low ($\simeq 0.02$), the fit indicates an oscillation of the polarization as a function of x_F with good $\chi^2/N_{DOF} = 0.81$. The data fits have been performed for ω parameter free (fit # 1) and $\omega = 22.27$ (fit # 2). Due to a limited statistics and kinematic range of the data, the η_1 parameter is fixed at the same value (0.31) as it is for Λ polarization in pA collisions. As we will see below the large value of $\omega = 18.5 \pm 5.7$ is typical for such exotic process ($p \rightarrow \bar{\Lambda}$) which corresponds to the $\Delta B = 2$ exchange, where B is a baryon number. The dependence of $\bar{\Lambda}$ polarization on x_F is shown in Fig. 17 along with fit # 2 predictions for $p_T = 0.8$ GeV/c and $p_T = 1.5$ GeV/c.

6.2. Polarization of $\bar{\Xi}^+$ in pA collisions

The $\bar{\Xi}^+$ polarization have been measured at 800 GeV/c in collisions of a proton beam with a Be target [21]. The data fits have been performed for ω parameter free (fit # 3), and $\omega = 65.19$ (fit # 4). The dependence of polarization on x_F is shown in Fig. 18 along with fit # 4 predictions for $p_T = 0.5$ GeV/c and $p_T = 1.5$ GeV/c. The value of $\omega = 64 \pm 22$ is very large. At the same time this value of ω is a minimal one which describes the unusual polarization dependence on x_F with the middle point closer to zero than the other ones. The fitting curves indicate that polarization magnitude could be about 0.18. If such an unusual behaviour will be confirmed by future experiments that reaction will be a large challenge to the strong interaction theory. Much more data are desirable since we have only 3 data points for this reaction.

6.3. The $\bar{\Lambda}$ polarization in $\bar{p}p$ collisions

The polarization of $\bar{\Lambda}$ ($\mathbf{P}_{\bar{\Lambda}}$) hyperons in $\bar{p}p$ collisions has been studied at 176 GeV/c [7]. The fit # 5 is made with ω parameter free, and the fit # 6 is made for $\omega = 14.21$. The dependence of $\mathbf{P}_{\bar{\Lambda}}$ on x_F is shown in Fig. 19 along with fit # 6 predictions for $p_T = 0.5$ GeV/c and $p_T = 1.5$ GeV/c, respectively. The predictions are made for 176 GeV/c $\bar{p}p$ collisions. Both fits indicate local maximums of $|\mathbf{P}_{\bar{\Lambda}}|$ at $x_F \approx 0.45$ and at $x_F \approx 0.65$ and an oscillation of $\mathbf{P}_{\bar{\Lambda}}$ as a function of x_F . An interesting feature of the data is that almost a full period of the oscillations is covered by the data. This observation needs additional conformation in different kinematic regions due to a limited statistics and the kinematic range covered by the data. Additional measurements are desirable to clarify the p_T dependence of the $\mathbf{P}_{\bar{\Lambda}}$.

The large values of ω have been found also for $pp(C) \rightarrow \bar{\Lambda} + X$ and for $pA \rightarrow \bar{\Xi}^+ + X$ reactions considered above. The dependence of the ω parameter on quantum numbers of the hadrons participating in the reaction will be discussed in details below.

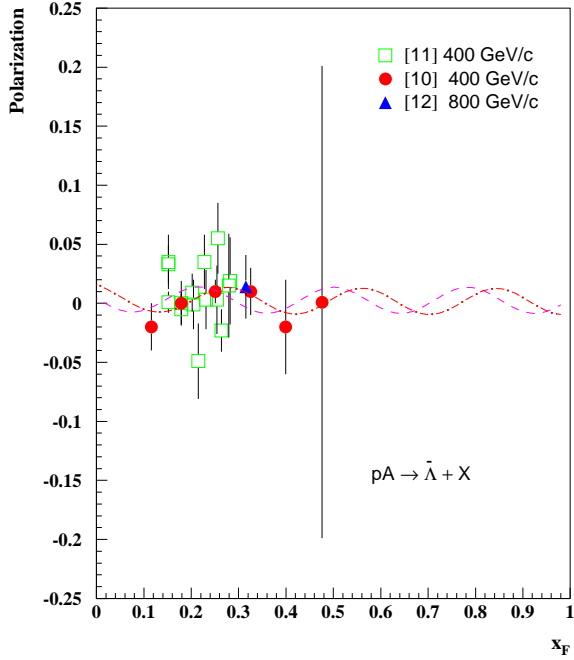


Fig. 17. Polarization vs x_F for $\bar{\Lambda}$ production in pBe collisions. The fit parameters of eqs. (10)-(19) are presented in Table 7. The curves correspond to the fit # 2 for $p_T = 0.8$ GeV/c (dashed), and $p_T = 1.5$ GeV/c (dash-dotted), respectively.

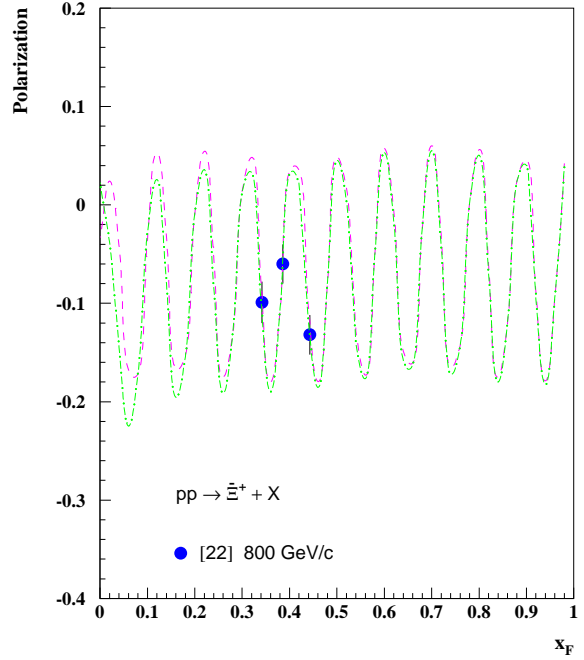
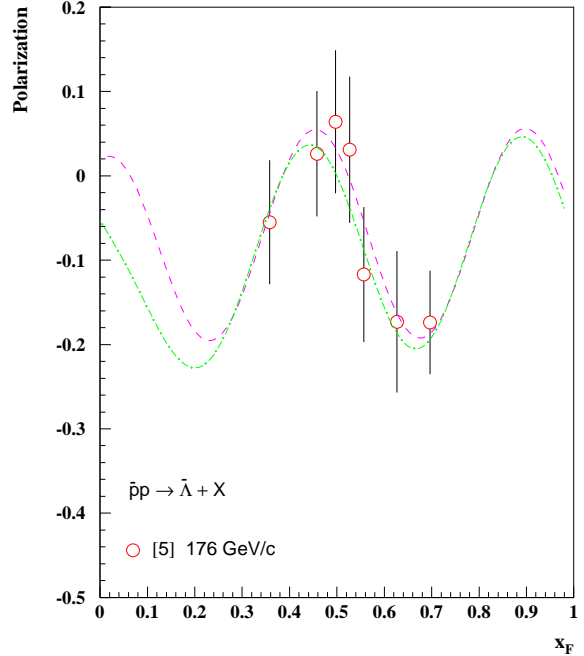


Fig. 18. Polarization vs x_F for $\bar{\Xi}^+$ production in pp collisions. The fit parameters of eqs. (10)-(19) are presented in Table 7. The curves correspond to the fit # 4 for $p_T = 0.5$ GeV/c (dashed), and $p_T = 1.5$ GeV/c (dash-dotted), respectively.

Fig. 19. Polarization vs x_F for $\bar{\Lambda}$ production in $\bar{p}p$ collisions. The fit parameters of eqs. (10)-(20) are presented in Table 7. The curves correspond to the fit # 6 for $p_T = 0.5$ GeV/c (dashed), and $p_T = 1.5$ GeV/c (dash-dotted), respectively.



6.4. Polarization of $\bar{\Sigma}^-$ in pCu collisions

The $\bar{\Sigma}^-$ polarization has been measured in the pCu collisions at 800 GeV/c [14]. The fit was not made since only four data points have been measured at fixed $x_F \approx 0.47$. The sign of polarization is positive and its magnitude is about 0.088 ± 0.011 .

7. Polarization of Ξ^- and Ω^- in collisions of hyperons and protons with nuclei

In this section we analyze the polarization of Ξ^- and Ω^- hyperons produced by a neutral unpolarized beam containing hyperons and the Ξ^- polarization produced by Σ^- beam. In addition, the Ω^- and the proton polarizations in $pp(A)$ collisions are analyzed and compared with the hyperon polarization in different reactions. The α parameter in eq. (10) is set to zero due to a limited number of used targets and statistics.

7.1. Polarization of Ξ^- in collisions of Λ and Ξ^0 with Be target

In this subsection we consider the data on Ξ^- polarization which have been measured using a neutral unpolarized high energy beam containing Λ and Ξ^0 hyperons [39]. The primary 800 GeV/c proton beam was used to produce a neutral strangeness containing beam, which in its turn interacted with a Be target. The average momentum of produced Ξ^- and Ω^- hyperons was about 395 GeV/c. This value of momentum was used to estimate the momentum of the neutral beam. It is assumed in this analysis that the ratio (R) of the neutral beam momentum to the 800 GeV/c primary momentum is the same as the ratio of Ξ^- momentum to the neutral beam momentum. These relations give $R = 0.703$ and the neutral beam momentum about $R \cdot 800 = 562$ GeV/c. Using this assumption we performed a fit of the data [39]. The fit parameters are presented in Table 8.

Table 8. Fit parameters of eqs. (10)-(20) for polarization of Ξ^- and Ω^- hyperons in collisions of a neutral unpolarized beam containing Λ and Ξ^0 with Be target, and the Ω^- polarization in pBe collisions.

Fit #	1	2	3	4
<i>Process</i>	$\Xi^0 \rightarrow \Xi^-$	$\Xi^0 \rightarrow \Xi^-$	$\Lambda \rightarrow \Omega^-$	$p \rightarrow \Omega^-$
c	2.37 ± 0.44	2.37 ± 0.42	2.6 ± 4.1	1.36 ± 0.69
ω	46.0 ± 3.7	45.97	6.090	22.27
σ	-1.0	-1.0	-1.0	1.0
p_T^0	1.0	1.0	1.0	0.39
η_0	0.151 ± 0.017	0.151 ± 0.003	0.24 ± 0.10	0.064 ± 0.012
η_1	0.0	0.0	0.0	0.0
δ	0.0	0.0	0.0	0.0
ξ_0	0.085 ± 0.023	0.085 ± 0.002	0.14 ± 0.03	0.372 ± 0.026
ξ_1	0.0	0.0	0.0	0.0
ν	0.0	0.0	0.0	0.0
χ^2/N_{DOF}	13.75/13	13.75/14	0.04/1	0.01/2

The polarization of Ξ^- was fitted with ω parameter free (fit # 1) and with $\omega = 45.97$ (fit # 2). The x_F dependence of polarization is shown in Fig. 20 along with the fit # 2 predictions for $p_T = 0.5$ GeV/c and $p_T = 1.5$ GeV/c. Though the magnitude of polarization ($\mathbf{P}_H^{\text{Max}}$) is about 0.026 only, a clear x_F dependence is seen, which is consistent with the oscillation behaviour, predicted by eqs. (10)-(20). The frequency parameter $\omega = 46.0 \pm 3.7$ is very large and an empirical relation for the polarization magnitude

$$|\mathbf{P}_H^{\text{Max}}| \approx 0.85/\omega \quad (21)$$

is valid. This relation is also confirmed above for Λ , Ξ^0 , and Ξ^- hyperons produced in pA collisions (see Tables 1 and 2). Relation (21) means that polarization for processes with large ω is expected to be low. We will see below that eq. (21) gives the right order of magnitude for most of the reactions but there are a few exclusions and a more complicated formula will be proposed below for the polarization magnitude.

7.2. Polarization of Ω^- in collisions of Λ and Ξ^0 with Be target

The Ω^- polarization has been measured using unpolarized neutral beam described in the previous subsection [39]. The polarization of Ω^- was fitted with $\omega = 6.090$ (fit # 3). The x_F dependence of polarization is shown in Fig. 21 along with fit # 3 predictions for $p_T = 0.5$ GeV/c and $p_T = 1.5$ GeV/c. The magnitude of Ω^- polarization is consistent with eq. (21).

7.3. Polarization of Ω^- in pBe collisions

The Ω^- polarization has been measured using 800 GeV/c pBe collisions for $0.3 < x_F < 0.7$ and $0.5 < p_T < 1.3$ GeV/c [40]. The mean value of polarization is -0.01 ± 0.01 , but the dependence of it on x_F clearly indicates its oscillation as a function of x_F (see Fig. 22). The fit # 5 is performed (see Table 8) with ω parameter fixed at 22.27 as is predicted by eq. (22). The magnitude of polarization oscillation is about 0.032 ± 0.016 .

7.4. Polarization of Ξ^- in collisions of Σ^- with $C(Cu)$ target

The polarization of Ξ^- has been measured using 330 GeV/c Σ^- beam on Carbon and Copper targets [41]. The polarization of Ξ^- for a sample, combining the C and the Cu target measurements, was fitted with free ω parameter (fit # 1) and with $\omega = 3.045$ (fit # 2). The fit parameters are presented in Table 9. The x_F dependence of polarization is shown in Fig. 23 along with fit # 2 predictions for $p_T = 0.5$ GeV/c and $p_T = 1.5$ GeV/c. The magnitude of Ξ^- polarization is consistent with eq. (21).

7.5. The proton polarization in $pp(C)$ collisions

It is interesting to compare the hyperon polarization data with the proton polarization data in $pp(C)$ collisions. The data have been measured at 100, 200, 300 and 400 GeV/c in collisions of a proton beam with protons and a Carbon target [42]. The data fits have been performed for ω parameter free (fit # 3) and $\omega = 6.090$ (fit # 4). The dependence of polarization on x_F is shown in Fig. 24 along with fit # 4 predictions for the proton and the Carbon targets. The p_T dependence of the polarization is mainly due to a significant p_T dependence of the phases x_1 and x_2 . The data are consistent with the scaling described by eq. (10) with $F(p_T)$ given by eq. (19).

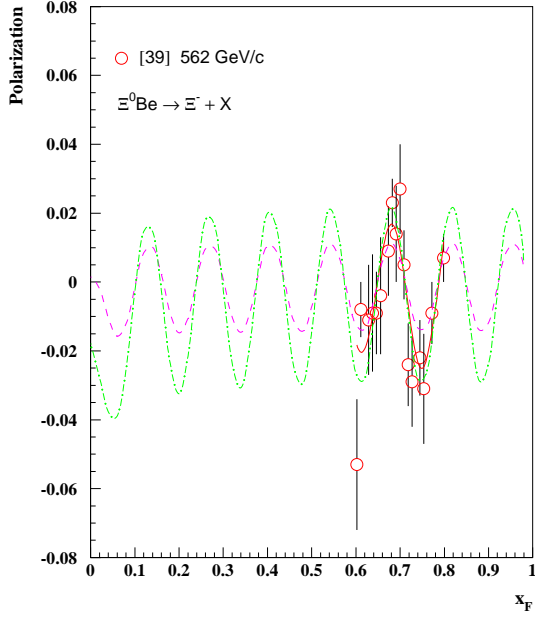


Fig. 20. Polarization vs x_F for Ξ^- production in $\Lambda(\Xi^0)p$ collisions. The fit parameters of eqs. (10)-(20) are presented in Table 8. The curves correspond to the fit # 2 for $p_T = 0.5$ GeV/c (dashed), and $p_T = 1.5$ GeV/c (dash-dotted), respectively.

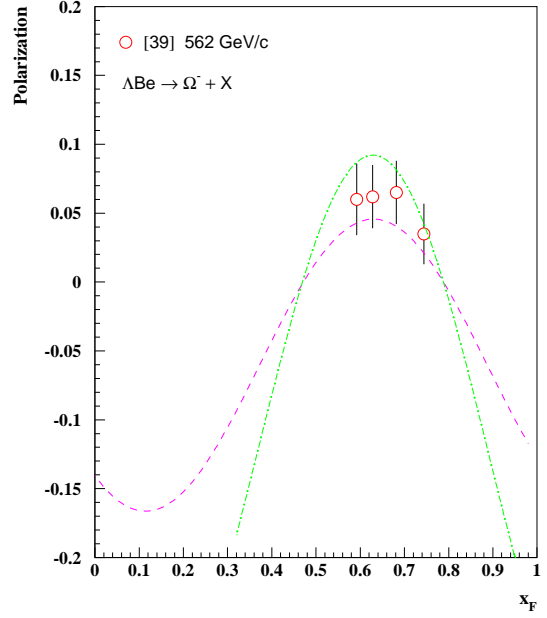


Fig. 21. Polarization vs x_F for Ω^- production in $\Lambda(\Xi^0)p$ collisions. The fit parameters of eqs. (10)-(20) are presented in Table 8. The curves correspond to the fit # 3 for $p_T = 0.5$ GeV/c (dashed), and $p_T = 1.5$ GeV/c (dash-dotted), respectively.

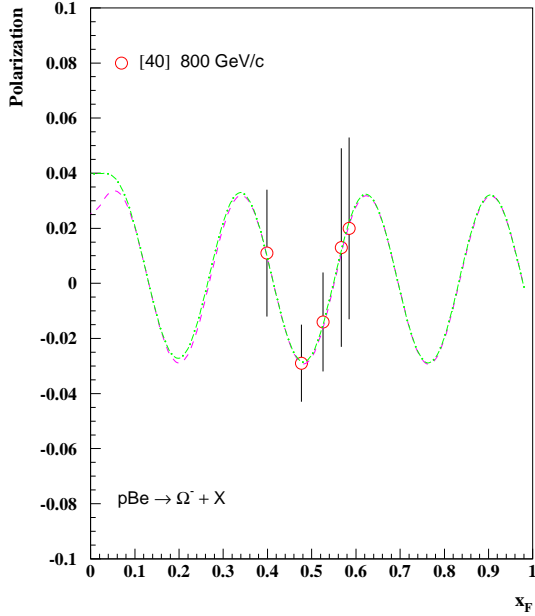


Fig. 22. Polarization vs x_F for Ω^- production in pBe collisions. The fit parameters of eqs. (10)-(19) are presented in Table 8. The curves correspond to the fit # 4 for $p_T = 0.5$ GeV/c (dashed), and $p_T = 1.0$ GeV/c (dash-dotted), respectively.

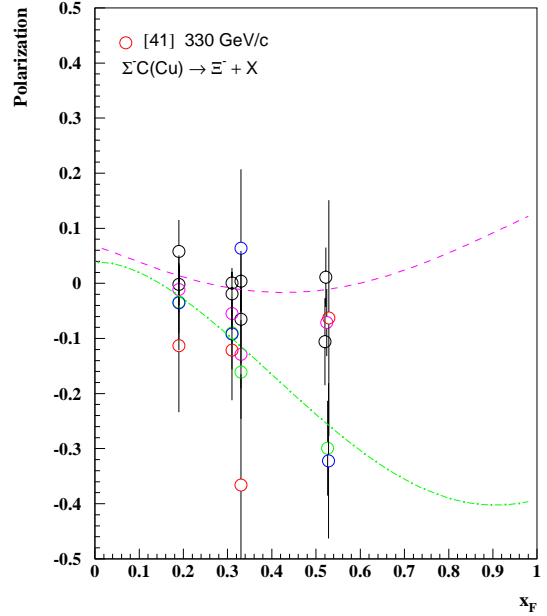


Fig. 23. Polarization vs x_F for Ξ^- production by Σ^- beam on $C(Cu)$ targets. The fit parameters of eqs. (10)-(20), are presented in Table 9. The curves correspond to the fit # 2 for $p_T = 0.5$ GeV/c (dashed), and $p_T = 1.5$ GeV/c (dash-dotted), respectively.

Fig. 24. Polarization vs x_F for proton production in $pp(C)$ collisions. The fit parameters of eqs. (10)-(19) are presented in Table 9. The curves correspond to the fit # 4 for $p_T = 0.5$ GeV/c and pp collisions (solid curve), $p_T = 1$ GeV/c and pC collisions (dashed curve).

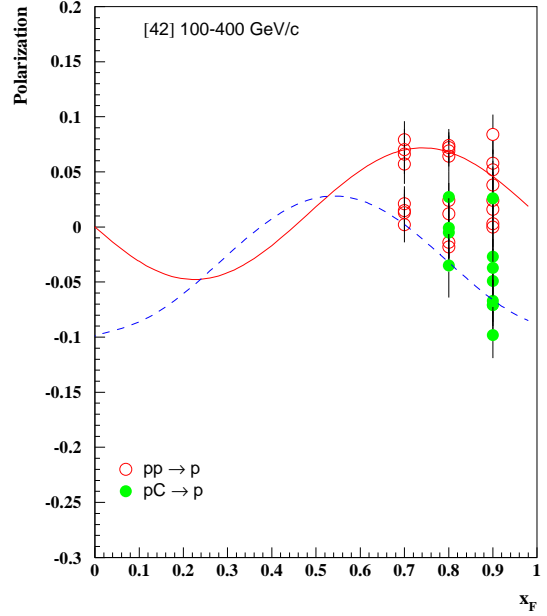


Table 9. Fit parameters of eqs. (10)-(20) for reactions $\Sigma^- + C(Cu) \rightarrow \Xi^- + X$ and $p(C) + p \rightarrow p + X$.

Fit #	1	2	3	4
<i>Process</i>	$\Sigma^- A \rightarrow \Xi^-$	$\Sigma^- A \rightarrow \Xi^-$	$pA \rightarrow p$	$pA \rightarrow p$
c	-1.53 ± 0.56	-1.51 ± 0.48	0.74 ± 0.14	0.73 ± 0.10
ω	3.3 ± 3.5	3.045	6.12 ± 0.21	6.090
σ	0.87 ± 0.27	0.88 ± 0.23	1.0	1.0
p_T^0	1.0	1.0	0.4	0.4
η_0	-0.41 ± 0.51	-0.446 ± 0.042	0.647 ± 0.014	0.648 ± 0.012
η_1	-0.20 ± 0.28	-0.21 ± 0.29	0.204 ± 0.045	0.205 ± 0.045
δ	4.6	4.6	1.75	1.75
ξ_0	0.84 ± 0.71	0.88 ± 0.23	1.474 ± 0.089	1.476 ± 0.090
ξ_1	0.71 ± 0.78	0.75 ± 0.34	1.75	1.75
ν	1.3	1.3	1.75	1.75
χ^2/N_{DOF}	10.7/17	10.7/18	35.9/31	35.9/32

8. Discussion

The results of the previous sections indicate that the use of two scaling variables $x_{A\pm} = (x_R \pm x_F)/2$ is essential for the universal energy independent description of the existing hyperon polarization data in inclusive reactions. The scaling variables transform into each other under rotation transformation around the normal to the scattering plane and allow one to satisfy in a natural way the feature (5), which is also related with the rotation invariance. The variables $x_{A\pm}$ treat on a more equal basis the data for the central and the fragmentation regions as well as the transverse and the longitudinal momentum components of the produced hyperon.

The form of eq. (10) is chosen from the dimensional analysis, the rotation invariance requirement and it is also motivated by the existing data for both the hyperon polarization and the analyzing power in inclusive reactions for hadron-hadron collisions. The derived formulas are applicable for both the A_N and the \mathbf{P}_H data approximation and reflect the scaling properties of these two classes of processes at high enough energies and p_T . The specific range of energies and p_T at which the scaling properties are valid could depend on the process type. The existence of the above scaling implies that large spin effects will survive at high energies and do not depend directly on the beam energy. These properties of the A_N and the \mathbf{P}_H are waiting for their explanation in the strong interaction theory in general and in the Quantum Chromodynamics (QCD) in particular.

8.1. Analogy between the scaling properties of hyperon polarization and the analyzing power

It is important to take into account in the future models a deep analogy between the hyperon polarization and the analyzing power, which follows from the results of this study and [47,48,49]. Below we list separately some features of the A_N and the \mathbf{P}_H , which in many aspects look very similar and indicate a common nature of both phenomena.

Features of the analyzing power in inclusive hadron production by polarized protons and antiprotons:

- a) Scaling behaviour for the analyzing power as a function of $x_{A+} = (x_R + x_F)/2$ and p_T in the polarized proton fragmentation region as well as in the central region.
- b) The analyzing power is approximated by a product of functions of p_T and x_{A+} : $A_N = F(p_T)G(x_{A+})$.
- c) The function $F(p_T)$ for analyzing power rises with p_T at small $p_T \leq p_T^0$ and have a plateau or decrease above p_T^0 , where $p_T^0 = 0.3-5$ GeV/c depends on a reaction type.
- d) The function $G(x_{A+})$ for the analyzing power is proportional to $\sin[\omega(x_{A+} - x_1)]$, where ω is a constant and x_1 could depend on p_T .
- e) The analyzing power is zero at $p_T = 0$ due to the absence of a preferable direction, such as a normal to the scattering plane. That implies $F(0) = 0$.
- f) $A_N \neq 0$ implies that the direction of transverse motion of the produced hadron depends on the polarization of the projectile.
- g) The sign and the magnitude of the A_N depend on the projectile, the target, and the produced hadron flavors. The same is valid for the parameters of equations, describing the scaling properties of A_N .

Features of the hyperon polarization in inclusive production by the pions, kaons, unpolarized protons, hyperons and antiprotons:

- a) Scaling behaviour for the hyperon polarization as a function of $x_{A\pm} = (x_R \pm x_F)/2$ and p_T in the beam fragmentation region, the target fragmentation region as well as in the central region.
- b) The hyperon polarization is approximated by a product of functions of p_T and $x_{A\pm}$: $\mathbf{P}_H = F(p_T)[G(x_{A+} - x_2) - \sigma G(x_{A-} + x_2)]$, where the x_2 and the σ could depend on p_T and a reaction type.

- c) The function $F(p_T)$ for the hyperon polarization rises with p_T at small $p_T \leq p_T^0$ and have a plateau or decrease above p_T^0 , where $p_T^0 = 0.4-2$ GeV/c depends on a reaction type.
- d) The function $G(x_{A\pm})$ for the hyperon polarization is proportional to $\sin[\omega(x_{A\pm} - x_1)]$, where ω is a constant and x_1 could depend on p_T .
- e) The hyperon polarization is zero at $p_T = 0$ due to the absence of a preferable direction, such as a normal to the scattering plane. This implies $F(0) = 0$.
- f) $\mathbf{P}_H \neq 0$ means that there exists a correlation between the direction of transverse motion of the produced hyperon and the polarization of this hyperon.
- g) The sign and the magnitude of the \mathbf{P}_H depend on the projectile, the target, and the produced hadron flavors. The same is valid for the parameters of equations, describing the scaling properties of \mathbf{P}_H .

Comparing the items corresponding to the analyzing power features and those referring to the hyperon polarization, we are practically forced to accept the conclusion that A_N and \mathbf{P}_H are closely related to each other.

8.2. Dependence of the hyperon polarization on quantum numbers

The magnitude of hyperon polarization (\mathbf{P}_H^{\max}) varies significantly with the hyperon, the projectile and the target flavors and the target atomic weight. The values of \mathbf{P}_H^{\max} for different reactions were estimated for $x_F \geq 0$, where most of the data have been measured, using eqs. (10)-(20) and fit parameters, taken from Tables 1-9. The sign of the \mathbf{P}_H^{\max} is indicated the same as that for the experimental data if it does not vary in the mentioned above region, and \pm - otherwise. The results are presented in Table 10 for 22 different reactions.

It is easy to notice from Table 10 that there is a correlation between the value of \mathbf{P}_H^{\max} and the ω parameter for the corresponding reactions. The product of these two values, $|\mathbf{P}_H^{\max}| \cdot \omega$ varies much less than each value separately. We may conclude from Table 10 that at least for the reactions of Λ , Ξ^0 and Ξ^- production in pBe collisions the magnitude of their polarization can be approximated by a simple empirical relation (21).

There is also a very interesting feature of the hyperon polarization, related with the value of the parameter ω in eqs. (10)-(21). The results of the data fits indicate (see Table 10) that for the hyperon and antihyperon production in $pp(A)$, $K^\pm p$, $\pi^\pm p$, $\Sigma^- p$, $\Lambda(\Xi^0)p$, and $\bar{p}p$ collisions the ω parameter depends on flavors of the projectile, the produced hyperon and the target. It can be expressed for the reaction $a + b \rightarrow c^\dagger + X$ using the formula

$$\omega_Q = \sum_{i=1}^{i=4} a_i Q_i, \quad (22)$$

where Q_i depends on the quark content of hadrons participating in the reaction, and a_i are fit parameters. In particular,

$$Q_1 = |B_c| [n_q(a\bar{c}) + n_q^{ext}(a\bar{c})], \quad (23)$$

$$Q_2 = B_{a\bar{c}} \Psi(B_a) + 2\delta [n_q(a\bar{c}) - 6] \delta(B_{a\bar{c}}), \quad (24)$$

$$Q_3 = |B_a| |B_c| \{B_{b\bar{c}} + 2\delta [n_q(a\bar{c}) - 6] \delta(B_{b\bar{c}})\}, \quad (25)$$

$$Q_4 = |B_a| \delta(N_s^c - 2) \cos[n_q^s(a\bar{c})\pi/2] \sin[n_q(a\bar{c})\pi/4], \quad (26)$$

where

$$\Psi(n) = \begin{cases} n, & \text{if } n \neq 0; \\ 1, & \text{otherwise,} \end{cases} \quad (27)$$

and

$$\delta(x) = \begin{cases} 0, & \text{if } x \neq 0; \\ 1, & \text{otherwise.} \end{cases} \quad (28)$$

Table 10. The estimate of maximum in hyperon polarization magnitude using the fit parameters of eq. (10)-(20). The maximum is estimated for $x_F \geq 0$ region.

#	reaction	c	c_Q	ω	ω_Q	\mathbf{P}_H^{\max}	P_Q
1	$pBe \rightarrow \Lambda$	-1.22 ± 0.05	-1.21	3.13 ± 0.24	3.045	-0.272 ± 0.011	-0.271
2	$pBe \rightarrow \Xi^0$	-1.37 ± 0.61	-0.89	6.10 ± 0.92	6.090	-0.141 ± 0.052	-0.121
3	$pBe \rightarrow \Xi^-$	-0.81 ± 0.12	-0.88	5.95 ± 0.74	6.090	-0.140 ± 0.021	-0.119
4	$pBe \rightarrow \Sigma^+$	3.96 ± 0.85	3.27	1.9 ± 1.2	3.045	0.337 ± 0.076	0.409
5	$pBe \rightarrow \Sigma^-$	4.2 ± 4.2	4.31	6.1 ± 4.0	6.090	0.34 ± 0.26	0.470
6	$K^-p \rightarrow \Lambda$	4.25 ± 0.37	4.41	3.53 ± 0.22	3.58	0.61 ± 0.11	0.575
7	$K^-p \rightarrow \Xi^-$	6.8 ± 2.7	2.98	3.04 ± 0.88	3.58	0.53 ± 0.17	0.345
8	$K^+p \rightarrow \Lambda$	-2.4 ± 1.3	-2.20	4.4 ± 1.5	3.58	$\pm 0.23 \pm 0.15$	-0.287
9	$\pi^-p \rightarrow \Lambda$	-1.67 ± 0.59	-1.62	4.33 ± 0.94	3.58	$\pm 0.23 \pm 0.14$	-0.223
10	$\pi^+p \rightarrow \Lambda$	-2.5 ± 2.9	-1.62	5.2 ± 6.5	3.58	$\pm 0.14 \pm 0.17$	-0.223
11	$K^-p \rightarrow \bar{\Lambda}$	10 ± 10	2.62	5.55	5.55	0.42 ± 0.40	0.307
12	$K^+p \rightarrow \bar{\Lambda}$	3.9 ± 1.0	5.25	4.4 ± 1.9	5.55	0.78 ± 0.25	0.614
13	$pBe \rightarrow \bar{\Lambda}$	-0.49 ± 0.22	-0.76	18.5 ± 5.7	22.27	$\pm 0.021 \pm 0.010$	-0.017
14	$\bar{p}Be \rightarrow \bar{\Lambda}$	3.5 ± 1.2	2.44	16.2 ± 4.1	14.21	$\pm 0.187 \pm 0.046$	0.168
15	$pBe \rightarrow \bar{\Xi}^+$	-16 ± 12	-17.7	63.9 ± 22.2	65.19	-0.18 ± 0.03	-0.194
16	$\Xi^0 Be \rightarrow \Xi^-$	2.37 ± 0.42	2.14	46.0 ± 3.7	45.97	$\pm 0.026 \pm 0.005$	0.025
17	$\Sigma^- C \rightarrow \Xi^-$	-1.51 ± 0.48	-1.77	3.3 ± 3.5	3.045	-0.40 ± 0.40	-0.36
18	$\Lambda Be \rightarrow \Omega^-$	2.6 ± 4.1	1.56	6.090	6.090	0.111 ± 0.067	0.128
19	$pp \rightarrow p$	0.73 ± 0.10	0.73	6.12 ± 0.21	6.090	$\pm 0.072 \pm 0.014$	0.068
20	$pBe \rightarrow \Omega^-$	1.36 ± 0.69	1.58	22.27	22.27	0.032 ± 0.016	0.029
21	$pCu \rightarrow \bar{\Sigma}^-$		3.17		22.27	0.088 ± 0.011	0.086
22	$pBe \rightarrow \Sigma^0$		3.26		3.045	0.28 ± 0.13	0.41

In the above formulas $n_q(a\bar{c})$ is the minimal number of quarks in the $a\bar{c}$ system ($q\bar{q}$ pairs of the same flavor are cancelled, see quark diagram in Fig. 25). The $n_q^{ext}(a\bar{c})$ denotes additional (extra) quarks and antiquarks, produced in a process above the minimal level when a higher order quark level diagram is used, as in the case of the process $p + p \rightarrow p + X$. In the last mentioned process $n_q(a\bar{c}) = 0$, and we assume that the inclusive protons are produced via a single valence quark fragmentation. So, four additional quarks and antiquarks are produced in this process, similar to the case of $p + p \rightarrow \Xi^- + X$ process, shown in Fig. 25. For all other processes presented in Table 10 the $n_q(a\bar{c}) > 0$ and $n_q^{ext}(a\bar{c}) = 0$. The sum $[n_q(a\bar{c}) + n_q^{ext}(a\bar{c})]$ can also be considered as the number of spectator quarks in a process $a \rightarrow c$.

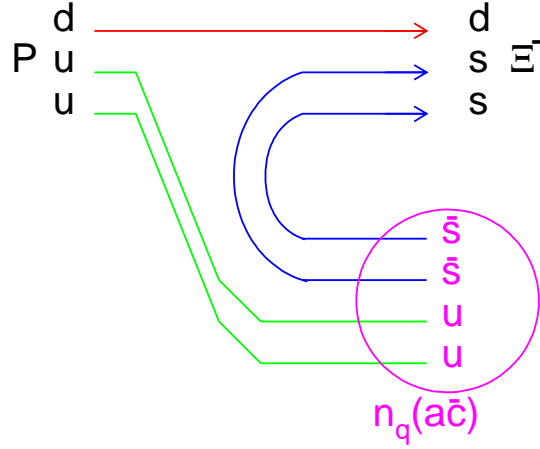


Fig. 25. The diagram of a proton fragmentation into a Ξ^- hyperon. The number of residual quarks is characterized by $n_q(a\bar{c})$.

The $n_q^s(a\bar{c})$ is the net number of s quarks or antiquarks in the $a\bar{c}$ system. The $B_{a\bar{c}}$ and $B_{b\bar{c}}$ are the baryon numbers of the $a\bar{c}$ and the $b\bar{c}$ systems, respectively. The B_a , B_b and B_c are the corresponding baryon numbers, and N_s^c is the number of s quarks in a produced hadron c .

The value $n_q(a\bar{c})$ is used in the Constituent Interchange model (CIM) [52] which predicts a cross section at $p_T = 0$ of the form

$$\frac{Ed^3\sigma}{d^3p}(a \rightarrow c) \sim (1 - x_F)^{2n_q(a\bar{c})-3}. \quad (29)$$

The first term of eq. (22) is needed to take into account the reactions # 1 - # 5, the second one takes into account the specific properties of the meson induced reactions # 6 - # 12, the third term is important for the antibaryon production, the Q_4 takes into account very high ‘‘oscillation frequency’’ data for the (anti)hyperons, containing *two* s quarks when the beam hadron has *two* (*zero*) s quarks (see reactions # 15-16).

The ω values presented in Table 10 were fitted using eq. (22) and the parameters a_i are shown in Table 11. The reactions #11,18 and 20-22 were not used in the fit, since they have too few data points.

Table 11. The fit parameters of eqs. (22), (33) and (39).

a_1	a_2	a_3	a_4	χ^2/N_{DOF}
1.523 ± 0.045	0.99 ± 0.24	5.58 ± 1.40	42.9 ± 3.7	3.57/13
b_1	b_2	b_3	b_4	χ^2/N_{DOF}
0.77 ± 0.41	0.48 ± 0.21	4.9 ± 4.1	12.8 ± 9.8	9.6/11
c_1	c_2	c_3	c_4	χ^2/N_{DOF}
2.0 ± 1.7	0.35 ± 0.51	5.9 ± 5.5	15.08 ± 9.7	5.77/12

If the inclusive protons are produced via the beam quark fragmentation similar to the reaction # 2, then the number of spectator quarks $n_q^{ext}(\bar{a}c) = 4$ and the predicted value $\omega_Q = 6.090$ is in a good agreement with the estimated value 6.12 ± 0.21 .

The dependence of the ω parameter vs ω_Q is shown in Fig. 26 for 17 different reactions, presented in Table 10. The arrow indicates also the position of the $\omega = 0.99$ prediction for the

analyzing power in the reactions $p^\dagger p \rightarrow \pi(K) + X$. The line in Fig. 26 shows the result of the fit $\omega = r \cdot \omega_Q$ with $r = 1.002 \pm 0.025$ and $\chi^2/N_{DOF} = 0.38/17$. This figure confirms a strong correlation of the ω parameter with the quantum numbers which characterize the reaction.

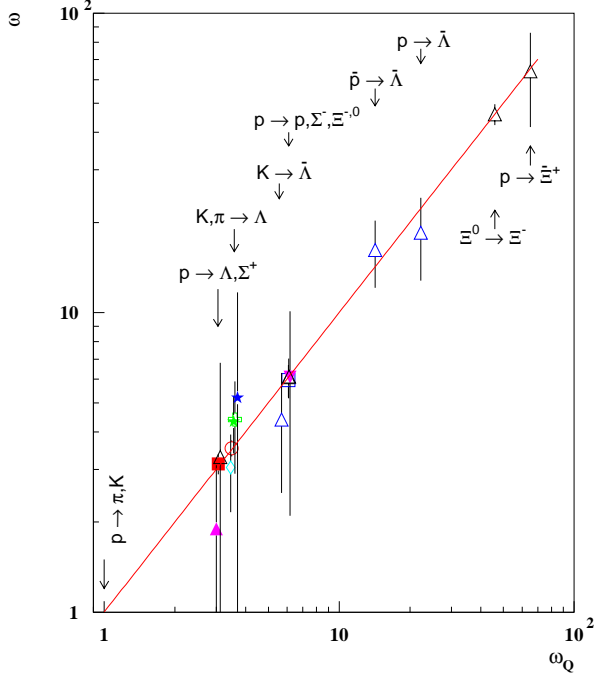


Fig. 26. The estimated ω parameter vs the predicted one, ω_Q .

The σ parameter was found to be consistent with

$$\sigma_Q = \begin{cases} 1, & \text{for } pp(A) \text{ collisions;} \\ -\Phi_Q, & \text{otherwise,} \end{cases} \quad (30)$$

where

$$\Phi_Q = (-1)^{n_c} \Psi(B_c) \Psi(Y_a) \Psi(Y_c) / \Psi(\Delta S_{ac}), \quad (31)$$

where Y_a , Y_c , and $\Delta S_{ac} = S_a - S_c$ are hypercharges ($Y = B + S$) of a , c , and strangeness change, respectively. The n_c is the number of quarks with parallel spins in the hadron c . It is assumed here, in accordance with the $SU(6)$ quark model [45,54], that $n_c = 3$ for the Ω^- , $n_c = 2$ for the $\Xi^{0,-}$, $\Sigma^{\pm,0}$, protons, neutrons, and $n_c = 1$ for the Λ .

The p_T^0 parameter was found to be consistent with an approximation

$$p_T^0 = k_T^0 / [n_q(a\bar{c}) + n_q^{ext}(a\bar{c})], \quad (32)$$

where $k_T^0 = 2.32 \pm 0.14$ GeV/ c .

The normalization parameter c in eq. (10) can be approximated by

$$c_Q = \frac{\epsilon_Q(\epsilon_a, \epsilon_b, \epsilon_c) \omega_Q \Phi_Q \Theta_Q V_Q W_Q(a_p, a_H)}{1 + \Delta\omega(\hat{b})}, \quad (33)$$

where

$$\epsilon_Q(\epsilon_a, \epsilon_b, \epsilon_c) = 3[\epsilon_a m_a / N_q^a + \epsilon_b m_b / N_q^b + \epsilon_c m_c / N_q^c] / m_p, \quad (34)$$

$$\Theta_Q = \{1 + 2\delta(B_{a\bar{c}})[\Psi(|B_{a\bar{b}}|) - 1]\} \{1 + S_a(1 - |B_a|)(1 + 3B_{b\bar{c}})/4\}, \quad (35)$$

$$V_Q = 1 + 4\delta(B_a - 1)\delta(S_c + 1)\delta(n_c - 2)/n_q(a\bar{c}), \quad (36)$$

$$W_Q(a_p, a_H) = [1 - a_p\delta(B_a - 1)\delta(S_a)]\exp\{a_H \sin[\pi(n_c - 1)|B_{a\bar{c}}||B_a|/4]\}. \quad (37)$$

The ratio $\Phi_Q/(1 + \Delta\omega(\hat{b}))$ takes into account the sign and the scale of polarization in the $x_F > 0$ region. The other factors in eq. (33) take into account the specific features of different reactions. The masses of the colliding hadrons are taken into account by a factor ϵ_Q , eq. (34), where m_a, m_b, m_c , and m_p are the masses of hadrons a, b, c and a proton, respectively. The N_q^a, N_q^b , and N_q^c are the numbers of quarks in the corresponding hadrons. Eq. (35) takes into account an enhanced polarization magnitude for the $\bar{p}p$ annihilation and for the strange meson induced reactions. The V_Q enhances the polarization in the hyperon beam induced reactions. The W_Q suppresses the hyperon polarization and enhances antihyperon polarization in the proton beam induced reactions. The last factor in the W_Q takes into account the enhanced polarization magnitude for antihyperons with $n_c = 2$ vs those with $n_c = 1$.

The value of $\Delta\omega(\hat{b})$ is given by eq.

$$\Delta\omega(\hat{b}) = \sum_{i=1}^{i=4} b_i Q'_i, \quad (38)$$

where $Q'_1 = |B_c|n_q^{ext}(a\bar{c})$, $Q'_2 = B_{a\bar{c}}\Psi(B_a)$, $Q'_3 = |B_a||B_c|B_{b\bar{c}}/\Psi[2(n_c - N_s^c) + 1]$, $Q'_4 = Q_4 B_c$, and b_i are the fit parameters. Eq. (33) has also five additional fit parameters: the normalization constants $\epsilon_a, \epsilon_b, \epsilon_c$, the a_p and the a_H parameters.

The fit of c parameter for the reactions #1 - # 19, presented in Table 10, is made using eq. (33). It gives $\epsilon_a = 0.49 \pm 0.14$, $\epsilon_b = 1.02 \pm 0.20$, $\epsilon_c = -0.76 \pm 0.15$, $a_p = 0.35 \pm 0.66$, and $a_H = 0.7 \pm 3.9$. The parameters b_i are presented in Table 11. The values of c_Q are presented in Table 10 with the sign given by eq. (33).

The magnitude \mathbf{P}_H^{\max} of the polarization can be approximated by the equation similar to eq. (33):

$$P_Q = A^\alpha \frac{\epsilon_Q(\epsilon'_a, \epsilon'_b, \epsilon'_c)\Phi_Q\Theta_Q V_Q H_Q W_Q(a'_p, a'_H)}{1 + \Delta\omega(\hat{c})}, \quad (39)$$

where

$$H_Q = (1 + |B_a|)\{1 - |B_{a\bar{c}}||B_a|/5\}/2. \quad (40)$$

The corresponding fit parameters ϵ'_a, \dots are different from ϵ_a, \dots due to non-zero phases x_1 and x_2 in eq. (10). The fit gives $\epsilon'_a = 0.55 \pm 0.22$, $\epsilon'_b = 1.47 \pm 0.37$, $\epsilon'_c = -1.10 \pm 0.25$, $a'_p = 0.34 \pm 1.04$, and $a'_H = 1.36 \pm 0.44$. The H_Q factor takes into account the suppression of hyperon polarization for meson induced reactions and a corresponding reduction of antihyperon polarization for baryon beams.

The dependence of α parameter in eq. (39) on quantum numbers is approximated as

$$\alpha_Q = \alpha_{eff} \cdot p_T^0 n_c / \Psi(|S_c|), \quad (41)$$

where $\alpha_{eff} = -0.22 \pm 0.05$.

The fit of $|\mathbf{P}_H^{\max}|$ using $|P_Q|$ (the sign of \mathbf{P}_H^{\max} was not taken into account) was made for the reactions # 1 - # 22. The resulting values of P_Q are shown in Table 10.

We can notice from Table 10 that eq. (39) predicts not only the right magnitude of the hyperon polarization but also predicts the right sign of it. In particular, for the reaction # 15, the Q'_4 and as a result the denominator are negative, that leads to the negative polarization sign

and a large magnitude of it. The sign of Q'_4 for the reaction # 16 is positive that results in a much smaller polarization magnitude. Both reactions (# 15 and # 16) represent unique cases of a very large "oscillation frequencies" ω and at the same time show significant polarization magnitudes. For the reaction # 15 the ω is larger by about 19 than it is for the reaction # 16 as we expect for antihyperon production, in analogy with the reactions # 13 and # 1.

Some predictions of the ω and other parameters of the hyperon polarization for the reactions not listed in Table 10 are shown in Table 12.

Table 12. The predictions of the ω and other parameters, characterizing hyperon polarization in different reactions.

#	reaction	ω_Q	c_Q	P_Q	α_Q	p_T^0
23	$\Xi^- p \rightarrow \Omega^-$	3.045	-2.2	-0.58	-0.25	1.16
24	$\Xi^0 p \rightarrow \Omega^-$	3.045	-2.2	-0.57	-0.25	1.16
25	$\Lambda p \rightarrow \Xi^-$	3.045	-1.6	-0.58	-0.25	1.16
26	$K^- p \rightarrow \Omega^-$	3.58	-0.53	0.047	-0.17	0.77
27	$\pi^+ p \rightarrow \bar{\Lambda}$	5.58	-0.88	-0.11	-0.17	0.77
28	$\pi^- p \rightarrow \bar{\Lambda}$	5.58	-0.88	-0.11	-0.17	0.77
29	$\bar{p} p \rightarrow \Lambda$	22.27	7.0	0.25	-0.08	0.39
30	$\bar{p} p \rightarrow \Sigma^+$	22.27	-13	-0.87	-0.16	0.39
31	$\bar{p} p \rightarrow \Xi^-$	65.19	2.0	0.033	-0.08	0.39

A new high statistics data are required for the reactions shown in Table 12 to establish their scaling properties and to estimate the ω parameter.

Eqs. (22), (33) and (39) should have their explanations in the models of strong interaction and ultimately in the QCD, perhaps, in the non-perturbative approach.

The value of parameter ω can also be estimated for the processes in which the analyzing power is measured. That requires additional precise measurements in a wide range of x_F in a kinematic area where the x_A scaling is fulfilled ($p_T \geq 1$ GeV/c and/or the beam energy ≥ 40 GeV). The reactions with meson beams are of special interest because of a high value of the ω parameter and a possibility of "oscillation" of the analyzing power as a function of x_F (compare Figs. 18-20, 22 and the preliminary results in [47]).

If we assume that eqs. (10)-(22) are valid also for the analyzing power A_N , we can make predictions of the ω for different reactions.

In particular, we expect $\omega = 0.99$ for the $\pi^{\pm,0}$, $K^{\pm,0}$, η production in pp and $\bar{p}p$ collisions; $\omega = 3.045$ for the Λ production in pp collisions; $\omega = 6.090$ for the proton production in pp collisions and $\omega = 22.27$ for the antiproton and $\bar{\Lambda}$ production in pp collisions. These predictions include 14 different reactions and are consistent with the data analysis presented in [48].

Eq. (22) also predicts that in some cases a target particle plays a significant role in the dynamics of a hyperon production. This is the case when the baryon number $B_{b\bar{c}}$ and Q_3 are different from zero.

The scaling behaviour of the A_N and \mathbf{P}_H indicates that the corresponding processes take place at the quark or parton level. In case of the discussed above scaling for the analyzing power and for the hyperon polarization such constituents could be the constituent quarks or

the current quarks (see related discussion in [55]). In order to resolve quark degrees of freedom inside a hadron, the transverse momentum p_T in a process should be higher than p_T^0 . That could be the reason for the p_T dependence of polarization (19).

8.3. Interference origin of the hyperon polarization

The polarization of hadrons is a pure Quantum mechanics effect related with the interference of spin-flip (g) and spin-nonflip (f) amplitudes. The transverse hadron polarization can be expressed via the f and g amplitudes as [56]

$$\mathbf{P}_H = \text{Im}(f^*g)/(|f|^2 + |g|^2). \quad (42)$$

Taking into account eqs. (10)- (12) we can choose amplitudes f and g as

$$f \propto f_0 \{ \exp[-i\omega(x_{A+} - x_1 - x_2)/2] + (\sqrt{\sigma})^* \exp[-i\omega(x_{A-} - x_1 + x_2)/2] \}, \quad (43)$$

$$g \propto g_0 \frac{c}{2\omega} A^{\alpha F}(p_T) \cdot \{ \exp[+i\omega(x_{A+} - x_1 - x_2)/2] - (\sqrt{\sigma}) \exp[+i\omega(x_{A-} - x_1 + x_2)/2] \}, \quad (44)$$

where f_0 and g_0 are the functions of kinematic variables (x_F , p_T , \sqrt{s}) with zero relative phases, which have to satisfy the constraints followed from both the polarization and the cross section data. The generalized optical theorem predicts the following relation for a cross section:

$$\mathbf{P}_H d\sigma = \text{Im}(f^*g), \quad (45)$$

where $d\sigma$ is the corresponding unpolarized inclusive cross section [46], which can be used together with eq. (42) to fix the f_0 and g_0 .

To have a non-zero value of the \mathbf{P}_H both amplitudes have to be non-zero and the phase difference $\Delta\phi$ between spin-flip and spin-nonflip amplitudes has to be non-zero too. For the cases of $\sigma = \pm 1$ the following phase differences are expected from eqs. (43)-(44):

$$\Delta\phi = (1 + \sigma)\pi/4 + \omega(x_R w_1 - x_1) + \text{Arg}(c/\omega). \quad (46)$$

As we can see from eq. (46), the variables x_R and ω play an important role in the hyperon polarization phenomena since they determinate the phase difference between the spin-flip and non-flip amplitudes. The higher is the ω value, the larger the $\Delta\phi$ change rate with the x_R increase. Eq. (22) for ω_Q can be considered as a sum of effective ‘‘charges’’, which create a mean field and lead to the change of the phase difference $\Delta\phi$.

In the lowest-order perturbative QCD all amplitudes are relatively real. This tends to rule out polarization in the hard scattering of partons, which seems to be well described in the low-order QCD . The observation of undiminished polarization near $p_T = 4$ GeV/c implies that either perturbative QCD does not apply or that another mechanism is responsible, such as interference of excited states or the fragmentation process [11].

8.4. Some theoretical ideas for hyperon polarization

Several phenomenological models have been proposed to explain the hyperon polarization data and the analyzing power data (see recent review in [46]). Some of the models have the features that allow one to understand, at least at a qualitative level, the analogy between the A_N and the \mathbf{P}_H discussed above.

8.4.1. Orbital motion of valence quarks

One class of such models assumes that an orbital motion of valence quarks and surface effects are responsible for the correlation between the quark spin direction and transverse motion of produced hadron [49,55]. By taking the Λ 's containing two, one or zero valence quark(s) of a beam proton into account, the model predicts the sign and the x_F dependence of Λ 's polarization. The model predicts correctly the sign and the magnitude of Σ^- , $\Xi^{0,-}$ polarization in pp collisions, and Λ polarization in K^-p collisions. It also predicts a smaller magnitude for Λ 's produced by π^\pm beams. The authors of the model claim an analogy of mechanisms, which lead to non-zero hyperon polarization and analyzing power. The model does not explain the specific features of antihyperon polarization.

8.4.2. Parton rotation inside constituent quarks

A separate approach was developed by Troshin and Tyurin, which assumes the rotation of a quark-antiquark cloud inside constituent quarks [57,58]. The main role belongs to the orbital angular momentum and polarization of the strange quark-antiquark pairs in the internal structure of constituent quarks. The hyperons are produced in two stages. At the first stage the overlapping and interaction of peripheral clouds occur which results in massive quark appearance and a mean field is generated. Constituent quarks located in the central part of hadron are supposed to scatter in a quasi-independent way by this mean field. At the second stage two mechanisms take place: Recombination of the constituent quarks with a virtual massive strange quark (soft interaction) into a hyperon or a scattering of a constituent quark in the mean field, excitation of this constituent quark, appearance of a strange quark as a result of decay of the constituent quark and a subsequent fragmentation of a strange quark into a hyperon (high p_T 's hard interaction). The resulting expression at $p_T > 1$ GeV/c is

$$P(s, x, p_T) \simeq \sin[P_q \langle L_{\bar{q}q} \rangle], \quad (47)$$

where P_q is the polarization of the constituent quark q which arises due to multiple scattering in the mean field and $\langle L_{\bar{q}q} \rangle$ is the mean value of an internal angular momentum inside the constituent quark.

Thus, in this model the polarization of a strange quark is the result of multiple scattering of a parent constituent quark, the correlation between the polarization of a strange quark and the polarization of the constituent quark and a local compensation of a spin and an orbital angular momentum of a strange quark.

The simplest possible x dependence of P_q is taken

$$P_q(x) = P_q^{max} x, \quad (48)$$

where $P_q^{max} = -1$.

The model predicts the negative sign and x_F dependence of the Λ polarization. Eq. (47) resembles eq. (12), especially in the beam fragmentation region. Eqs. (47), (48) predicts a scaling behaviour of the hyperon polarization. The concept of the mean field, generated by quarks, which leads to a hyperon polarization is also in consent with the analysis, presented above. There are no predictions for other hyperons, though the authors assume zero polarization in inclusive process $pp \rightarrow p + X$ due to a low probability of multiple scattering in the mean field in comparison with a single scattering. A single scattering does not polarize quarks and protons appear unpolarized in the final state since a single scattering is dominant in this process.

There are several semiclassical models, which provide simple arguments for a qualitative description of the hyperon polarization, but since they fully ignore the relevance of the phase difference, which is crucial, they are unable to make solid quantitative predictions.

8.4.3. The recombination model

In the recombination model [59,60] a dynamical reason for the above mentioned spin-momentum correlation is explained by the effect of Thomas precession [61,62]. The effect arises when the direction of the force acting on a quark does not coincide with the direction of its motion. It leads to a rotation of the quark spin and could be the reason of the discussed above “oscillation” of polarization or analyzing power as a function of x_F . The Thomas frequency is an inverse function of a quark mass

$$\vec{\omega}_T = \frac{\gamma}{\gamma + 1} \frac{\vec{F}}{m_q} \times \vec{V}, \quad (49)$$

where V is the strange quark velocity, F - the force, m_q - the strange quark mass, and $\gamma = (1 - V^2)^{-1/2}$. An additional term will appear in the effective Hamiltonian which describes the recombination process

$$U = \vec{S} \cdot \vec{\omega}_T, \quad (50)$$

where \vec{S} is a spin of the quark. Within the old-fashioned perturbation theory the final expression for the Λ polarization is

$$P(p \rightarrow \Lambda) = -\frac{12p_T x_F (x_F - 3x_s)}{\Delta x_0 M^2 (x_F + 3x_s)^2}, \quad (51)$$

where it is assumed that a recombination (hadronization) time $\Delta t \propto (p_z^{ave}/m_q)\Delta x_0$, the average momentum of the quark is $p_z^{ave} \propto P(x_F + 3x_s)/6$ and $\Delta x_0 \approx 4 \text{ GeV}^{-1}$ is a distance scale of the order of the proton radius. The $M \simeq 2 \text{ GeV}/c^2$ is an effective mass and the x_s is a fraction of a proton momentum (P) which carries the s quark [59]. These assumptions lead to a quark mass cancellation in the polarization formula (51) and a scaling behaviour of the Λ polarization. The model gives the right sign and a good approximation of the x_F dependence for the Λ polarization. There are also many predictions for hyperon polarization in other reactions. They are based on some rules which are formulated within the framework of the recombination model. In particular, there is a statement that the effect of recombination of the partons in the proton as they are transferred into the outgoing hadron may be different depending on whether they are accelerated (as are the slow sea partons) or decelerated (as are the fast valence partons). It is also a statement that two partons with similar wave functions in the proton may interact with themselves differently not as they interact with a parton whose wave function is different. This results in a simple rule: Slow partons preferentially recombine with their spins down in the scattering plane while fast partons recombine with their spins up.

The model predicts correctly the polarization sign but not the magnitude for some of the reaction. So, the model predicts the same polarization magnitude for $p \rightarrow \Lambda$ as it is for $p \rightarrow \Xi^{-,0}$, but we know from the above analysis that the polarization magnitudes for $\Xi^{-,0}$ are two times smaller. Similarly, for $K^- p \rightarrow \Lambda$ process the model predicts the same magnitude as for $p \rightarrow \Lambda$, while the measured value is two times larger. Since the polarization in the model is essentially kinematic at the quark level all the antibaryons should have zero polarization. As we have seen in the above analysis, the experimental situation is much more complicated.

There is another estimate of the hadronization time which follows from the analysis of A -dependence of hadron production $\Delta t \approx p^c/M_0^2$, where $M_0 \approx 1$ GeV [63]. The use of this Δt estimate results in a different expression for the Λ polarization

$$P(p \rightarrow \Lambda) = -\frac{2p_T M_0^2 x_F (x_F - 3x_s)}{m_q M^2 x_R (x_F + 3x_s)}, \quad (52)$$

which is an inverse function of the s quark mass m_q . This example shows that the hyperon polarization is sensitive to the details of the hadronization process. These results seem to imply that the origin of hyperon polarization is closely related with the confinement mechanism.

Since the Thomas precession frequency is an inverse function of the quark mass m_q , this may be the reason for a large variation of the ω_Q parameter for different reactions. The ratio m_s/m_d is estimated to be from 17 to 25 with a mean about 21 [64]. The same order of magnitude is given by the ratio $65.19/3.045 = 21.4$ of the ω_Q parameters for the processes $p \rightarrow \Xi^+$ and $p \rightarrow \Lambda$, in which s and \bar{d} quarks play an important role. It is interesting to estimate the number of revolutions of a quark spin using the above approximations

$$N_{rot} = \omega_T \Delta t \approx \frac{p_T \cdot (x_F - 3x_s)}{m_q \cdot (x_F + 3x_s)}. \quad (53)$$

Taking typical $x_F = 0.7$, $x_s = 0.1$, $p_T = 1$ GeV/c, and $m_s = 122$ MeV/c², we have $N_{rot} = 3.3$, while for the d quark with $m_d = 6$ MeV/c² the $N_{rot} = 67$. So, the number of quark spin revolutions due to the Thomas precession could be rather large and varies in the same range as that of the ω_Q .

8.4.4. Lund model

Another explanation of spin-momentum correlation follows from a picture of a colour flux tube, which emerges after the collision between an outgoing quark and the rest of hadronic system [65,66]. The $SU(6)$ wave function is assumed for hadrons, in particular, for Λ the (ud) system is in a singlet state, so the Λ polarization is that of the s quark. An outgoing ud diquark with spin $S = 0$ and isospin $I = 0$ stretches the color field and a $s\bar{s}$ pair is produced. It is assumed that the s quark has p_T which must be locally compensated by that of the \bar{s} quark. As a result, the $s\bar{s}$ pair has an orbital momentum which is assumed to be balanced by the spin of the $s\bar{s}$ pair. The model predicts a negative Λ polarization in pp collisions but cannot predict its magnitude or x_F dependence. The p_T dependence of the polarization is linear. The model needs additional assumptions to explain the polarization in other reactions and fails to explain the antihyperon polarization.

8.4.5. Optical approximation

We propose a simple toy model which uses an analogy with the optics. Let us consider the Ξ^- production in a collision of two protons (a and b) in their c.m. reference frame. The proton's longitudinal size is about $2R_h/\gamma_{cm}$, where $R_h \approx 0.8$ fm is a proton radius and $\gamma_{cm} = E_{cm}/(2m_p c^2)$.

In an optical picture the phase can be related with the number of scattering centers [67]. We assume here that a hadron can be characterized by an effective refractive index (n) which leads to a phase difference $\chi = (n-1)d \cdot p_q/\hbar$ between spin-flip and spin-nonflip quark scattering

amplitudes, where d is a total path length inside a proton and $p_q \approx p_c/z \approx p_a x_R/z$ is a quark momentum. It is assumed here for the sake of simplicity that a quark from the proton a passes on average half of the proton b thickness and then changes its angle due to a scattering in the proton b . The second part of its way inside the proton is approximately by a factor of $1/\cos\theta_{cm} = x_R/x_F$ larger than that before the scattering (we consider here not too large scattering angles). This results in a phase difference

$$\chi_a \approx \frac{R_h(n-1)x_R}{\lambda_p \langle z \rangle x_F} (x_F + x_R), \quad (54)$$

where $\lambda_p = \hbar/(m_p c) \approx 0.210$ fm is the proton Compton wavelength. Eq. (54) can be rewritten as $\chi_a = \omega_{eff} \cdot x_{A+}$, where

$$\omega_{eff} = \frac{2R_h(n-1)x_R}{\lambda_p \langle z \rangle x_F}, \quad (55)$$

and $\langle z \rangle$ is the mean fraction of quarks momentum which is carried by the produced hyperon. A similar consideration of the proton b quark scattering inside the proton a results in a $\chi_b = \omega_{eff} \cdot x_{A-}$ and the total contribution into the Ξ^- polarization is

$$\mathbf{P}_{\Xi^-} \propto [\sin(\omega_{eff} \cdot x_{A+}) - \sin(\omega_{eff} \cdot x_{A-})], \quad (56)$$

which is very similar to eq. (10). The averaging over the transverse quark coordinates inside a proton is not taken into account for the sake of simplicity. A more careful consideration of a quark path length after the scattering removes the singularity $1/x_F$ in eq. (56) since the path length is limited at $\theta_{cm} = \pi/2$ by the R_h . The p_T dependence of a hyperon polarization is also not taken into account in eq. (56) since we assume that p_T is high enough to resolve quarks inside the hadron structure. The condition for that is $p_T \cdot R_h \gg \hbar$, or $p_T \gg 0.25$ GeV/c. Comparison of eqs. (55) and (22) assumes that $(n-1) \propto \omega_Q \propto n_q(a\bar{c})$.

We may learn from this toy model that the hyperon polarization oscillation is probably related with a corresponding scattering amplitude phase change due to the hadron mean field generated during hadron interaction. The scaling variables x_{A+} and x_{A-} arise in this model from the consideration of geometrical and relativistic properties of hadrons interaction and the assumption that the phase difference χ is proportional to the quark path length in the mean hadron field.

Conclusion

It is shown that the existing hyperon polarization data in inclusive reactions for $pp(A)$, $\pi^\pm p$, $K^\pm p$, $\bar{p}p$ and hyperon-nucleon collisions can be described by a simple function of p_T and two scaling variables $x_{A\pm} = (x_R \pm x_F)/2$: $\mathbf{P}_H = A^\alpha F(p_T)[G(x_{A+} - x_2) - \sigma G(x_{A-} + x_2)]$. It can be presented also for the case of $pp(A)$ collisions as a product of functions of p_T , x_R , and x_F

$$\mathbf{P}_H = \frac{c}{\omega} A^{\alpha_1 |x_F|} \cdot F(p_T) \cos[\omega(x_R/2 - x_1)] \sin[\omega(x_F/2 - x_2)], \quad (57)$$

where $F(p_T)$, x_1 , and x_2 are the functions of p_T , which can be approximated by constants above 1-2 GeV/c, depending on a reaction type. The data fits indicate a simple relation for the ω parameter in case of hyperons produced in pp collisions: $\omega \approx 1.5n_q(a\bar{c})$, where $n_q(a\bar{c})$ is the number of quarks in the $a\bar{c}$ system. This relation and the data fits allow one to predict a

maximum in the absolute value of hyperon polarization at $x_F \approx 0.6 - 0.9$ for $\omega \approx 3$ (Λ and Σ^+), and at $x_F \approx 0.3 - 0.6$ for $\omega \approx 6$ (Σ^- , Ξ^- , and Ξ^0). To describe the ω also for the antihyperon polarization as well as for the hyperon polarization in collisions different from pp , additional terms are needed which are presented in eq. (22).

The p_T dependence of hyperon polarization not related with scaling variables $x_{A\pm}$, is given by the $F(p_T)$, which is rising at small p_T and probably have a plateau above 0.4-2.0 GeV/c, depending on the reaction type. No evidence of the decrease of the $F(p_T)$ at high p_T is found.

The data fits indicate also that the Λ hyperon polarization decreases on nuclear targets according to the law $\mathbf{P}_H \propto A^{\alpha_1|x_F|}$, with $\alpha_1 \approx -0.16$. This effect may be related with the rescattering of polarized s quarks in the nuclear matter before formation of a hyperon is over. Since the formation length is proportional to the final hyperon momentum, we expect a rise of s quark rescattering probability with $|x_F|$ increase. Due to the similarity between the hyperon polarization and the analyzing power scaling features we expect that the A -dependence of the analyzing power is also described by the law $A_N \propto A^{\alpha_1|x_F|}$ with $\alpha_1 \approx -(0.1 \div 0.3)$.

The polarization of Λ and Ξ^- in K^-p collisions has the same sign and order of magnitude. The maximum of polarization is located near $x_F = 0.6 - 0.7$. The corresponding ω parameter in eq. (10), which determines the rate of polarization change when x_F increases, is close to 3.5 for both reactions.

The sign of the polarization for a hyperon which have common valence quarks with the beam hadron is in accordance with the known rule that a valence quark scattered to the left prefers to have a positive polarization. Such behaviour is in a qualitative agreement with the predictions from the models, which take into account the Thomas precession [59,60] and color forces between an outgoing quark and the rest of hadronic system [65,66].

The polarization of $\bar{\Lambda}$ in $\bar{p}p$ collisions is fitted well by eq. (10) and indicates an oscillation of it as a function of x_F . Similar oscillations with high ω parameter are also seen for other processes, including $\Xi^0 \rightarrow \Xi^-$ and $p \rightarrow \Omega^-$.

A universal description of the hyperon polarization in all hadron induced reactions is proposed, which also includes the antihyperon production. The polarization sign, its magnitude as well as the ω parameter depend on quark composition of hadrons participating in the reaction and can be predicted using the proposed formulas.

There is an analogy between the scaling properties of polarization for hyperons, produced in collisions of unpolarized hadrons, and the scaling properties of the analyzing power of hadrons, produced in the collisions of polarized protons (antiprotons) with hadrons. Both spin-dependent quantities can be approximated as a product of a function $F(p_T)$ and a function of scaling variables $x_{A\pm}$: $G(x_{A+})$ in the case of analyzing power, and $[G_+(x_{A+}) - G_-(x_{A-})]$ in the case of hyperon polarization. The functions $G(x_{A+})$ or $G_{\pm}(x_{A\pm})$ are approximated in the scaling limit by a simple expression $\propto \sin[\omega(x_{A\pm} - x_1)]$, where x_1 can be a constant or a function of p_T . This analogy between the analyzing power and the hyperon polarization indicates on a common origin of both phenomena.

References

- [1] Bunce G. et al. // Phys. Rev. Lett. 1976, v. 36, p. 1113.
- [2] Abe F. et al. // Phys. Rev. 1986, v. D34, p. 1950.
- [3] Abe F. et al. // Phys. Rev. Lett. 1983, v. 50, p. 1102.

- [4] Bonner B.E. et al. // Phys. Rev. 1988, v. D38, p. 729.
- [5] Dukes E.C. et al. // Phys.Lett. 1987, v. B193, p. 135.
- [6] Raychaudhuri K. et al. // Phys. Lett. 1980, v. 90B, p. 319.
- [7] Gourlay S.A. et al. // Phys. Rev. Lett. 1986, v. 56, p. 2244.
- [8] Wilkinson C. et al. // Phys. Rev. Lett. 1981, v. 46, p. 803.
- [9] Heller K. et al. // Phys. Rev. Lett. 1983, v. 51, p. 2025.
- [10] Heller K. et al. // Phys. Rev. Lett. 1978, v. 41, p. 607.
- [11] Lundberg B. et al. // Phys. Rev. 1989, v. D40, p. 3557.
- [12] Ramberg E.J. et al. // Phys. Lett. 1994, v. 338B, p. 403.
- [13] Smith A.M. et al. // Phys. Lett. 1987, v. 185, p. 209.
- [14] Morelos A. et al. // Phys. Rev. Lett. 1993, v. 71, p. 2172.
- [15] Wilkinson C. et al. // Phys. Rev. Lett. 1987, v. 58, p. 855.
- [16] Ankenbrandt C. et al. // Phys. Rev. Lett. 1983, v. 51, p. 863.
- [17] Wah Y.W. et al. // Phys. Rev. Lett. 1985, v. 55, p. 2551.
- [18] Deck L. et al. // Phys. Rev. 1983, v. D28, p. 1.
- [19] Bonner B.E. et al. // Phys. Rev. Lett. 1989, v. 62, p. 1591.
- [20] Duryea J. et al. // Phys. Rev. Lett. 1991, v. 67, p. 1193.
- [21] Ho P.M. et al. // Phys. Rev. Lett. 1990, v. 65, p. 1713.
- [22] Trost L.H. et al. // Phys. Rev. 1989, v. D40, p. 1703.
- [23] Rameika R. et al. // Phys. Rev. 1986, v. D33, p. 3172.
- [24] Faccini-Turler M.L. et al. // Z. Phys. 1979, v. C1, p. 19.
- [25] Borg A. et al. // Nuovo Cimento 1974, v. 22A, p. 559.
- [26] Abramowicz H. et al. // Nucl. Phys. 1976, v. B105, p. 222.
- [27] Grassler H. et al. // Nucl. Phys. 1978, v. B136, p. 386.
- [28] Baubillier M. et al. // Nucl. Phys. 1979, v. B148, p. 18.
- [29] Bensinger J. et al. // Nucl. Phys. 1985, v. B252, p. 561.
- [30] Ganguli S.N. et al. // Nucl. Phys. 1977, v. B128, p. 408.
- [31] Chliapnikov P.V. et al. // Nucl. Phys. 1976, v. B112, p. 1.

- [32] Barletta W. et al. // Nucl. Phys. 1973, v. B51, p. 499.
- [33] Ajinenko I.V. et al. // Phys. Lett. 1983, v. 121B, p. 183.
- [34] Adeva B. et al. // Z. Phys. 1984, v. C26, p. 359.
- [35] Sugahara R. et al. // Nucl. Phys. 1979, v. B156, p. 237.
- [36] Barreiro F. et al. // Phys. Rev. 1978, v. D17, p. 669.
- [37] Bensinger J. et al. // Phys. Rev. Lett. 1983, v. 50, p. 313.
- [38] Stuntebeck P.H. et al. // Phys. Rev. 1974, v. D9, p. 608.
- [39] Heller K. - In Proceedings of the 12th International Symposium on High-Energy Spin Physics, September 10 - 14, 1996. Amsterdam, The Netherlands. Ed. by C.W. de Jager et al. (World Sci., Singapore. 1997), p. 23.
- [40] Luk K.B. et al. // Phys. Rev. Lett. 1993, v. 70, p. 900.
- [41] Adamovich M.I. et al. // Z. Phys. 1995, v. A350, p. 379.
- [42] Polvado R.O. et al. // Phys. Rev. Lett. 1979, v. 42, p. 1325.
- [43] Kane G.L., Pumplin J. and Repko W. // Phys. Rev. Lett. 1978, v. 41, p. 1689.
- [44] Pondrom L.G. // Phys. Rep. 1985, v. 122, p. 57.
- [45] Lach J. - Hyperon Polarization and Magnetic Moments. Preprint FERMILAB-Conf-93/381, Batavia, 1993.
- [46] Soffer J. - Is the riddle of the hyperon polarization solved?, Marseille preprint CPT-99-P-3898, Sep. 1999. Invited talk at Hyperon 99: Hyperon Physics Symposium, Batavia, Illinois, 27-29 Sep. 1999. p. 121. hep-ph/9911373 (1999).
- [47] Abramov V.V. - A New Scaling for Single-Spin Asymmetry in Meson and Baryon Hadroproduction. IHEP Preprint 98-84, Protvino, 1998.
- [48] Abramov V.V. // Eur. Phys. J. 2000, v. C14, p. 427.
- [49] Liang Zuo-tang and Boros C. // Phys. Rev. Lett. 1997, v. 79, p. 3608.
- [50] Bushnin Yu. et al. // Phys. Lett. 1969, v. 29, p. 48.
- [51] Felix J. et al. // Phys. Rev. Lett. 1996, v. 76, p. 22.
- [52] Blankenbecker R. and Brodsky S.J. // Phys. Rev. 1974, v. D10, p. 2973.
- [53] Qui J. and Sterman G. // Phys. Rev. 1999, v. D59, p. 014004.
- [54] Franklin J. // Phys. Rev. 1968, v. 172, p. 1807.
- [55] Boros C., Liang Zuo-tang // Phys. Rev. 1998, v. D57, p. 4491.

- [56] Ryskin M.G. - Polarization phenomena and confinement forces, In Proc. of the Int. Conf. on Quark Confinement and the Hadron Spectrum, Como, Italy, 20-24 June 1994. Edited by N.Brambilla and G.M.Prosperi. River Edge, N.J., (World Scientific, 1995), p. 261.
- [57] Troshin S.M. and Tyurin N.E. // Phys. Rev. 1997, v. D55, p. 1265.
- [58] Troshin S.M. and Tyurin N.E. // Phys. Rev. 1995, v. D52, p. 3862.
- [59] DeGrand T.A., Miettinen H. // Phys. Rev. 1981, v. D24, p. 2419.
- [60] DeGrand T.A. et al. // Phys. Rev. 1985, v. D32, p. 2445.
- [61] Thomas L.T. // Philos. Mag. 1927, v. 3, p. 1.
- [62] Logunov A.A. - On Tomas Precession. IHEP preprint 98-85, Protvino, 1998.
- [63] Abramov V.V. // Yad. Fiz. 1986, v. 44, p. 1318. [Sov. J. Nucl. Phys. 1986, v. 44, p. 856].
- [64] Groom D.E. et al. // Eur. Phys. J. 2000, v. C15, p. 1.
- [65] Anderson B., Gustafson G. and Ingelman G. // Phys. Lett. 1979, v. B85, p. 417; Phys. Rep. 1983, v. 97, p. 31.
- [66] Ryskin M.G. // Yad. Fiz. 1988, v. 48, p. 1114.
- [67] Troshin S.M., Tyurin N.E. // Uspechi Fiz. Nauk 1994, v. 164, p. 1073.

Received March 13, 2001

В.В. Абрамов

Универсальное скейлинговое поведение поперечной поляризации для инклюзивного образования гиперонов в адрон-адронных соударениях.

Оригинал-макет подготовлен с помощью системы L^AT_EX.

Редактор Е.Н.Горина.

Технический редактор Н.В.Орлова.

Подписано к печати 16.03.2001. Формат 60 × 84/8. Офсетная печать.

Печ.л. 5.12. Уч.-изд.л. 4.1. Тираж 160. Заказ 73. Индекс 3649.

ЛР №020498 17.04.97.

ГНЦ РФ Институт физики высоких энергий
142284, Протвино Московской обл.

